Title: Intermittent fasting promotes type 3 innate lymphoid cells secreting IL-22 contributing to the beigeing of white adipose tissue.

Running Title: type 3 innate lymphoid cells and beigeing

Authors: Hong Chen[1,4#], Lijun Sun[1#], Lu Feng[1], Xue Han[1], Yunhua Zhang[1], Wenbo Zhai[1], Zehe Zhang[1], Michael Mulholland[2], Weizhen Zhang[1,2*], Yue Yin[3*]

Affiliations:

1. Department of Physiology and Pathophysiology, School of Basic Medical Sciences, and Key Laboratory of Molecular Cardiovascular Science, Ministry of Education, Peking University, Beijing 100191, China
2. Department of Surgery, University of Michigan Medical Center, Ann Arbor, MI 48109-0346, USA
3. Department of Pharmacology, School of Basic Medical Sciences, and Key Laboratory of Molecular Cardiovascular Science, Ministry of Education, Peking University, Beijing,100191, China.
4. State Key Laboratory of Female Fertility Promote, Center for Reproductive Medicine, Department of Obstetrics and Gynecology, Peking University Third Hospital, Beijing, China.

# These authors contribute equally to the study

***Correspondence:**

Weizhen Zhang

Department of Physiology and Pathophysiology, School of Basic Medical Sciences, Peking University Health Science Center, Beijing 100191, China

E-mail: weizhenzhang@bjmu.edu.cn; Tel: 0086-10-82802183

or

Yue Yin

Department of Pharmacology, School of Basic Medical Sciences, and Key Laboratory of Molecular Cardiovascular Science, Ministry of Education, Peking University, Beijing,100191, China.

E-mail: yueyin@bjmu.edu.cn; Tel: 0086-10-82802514

Author contributions

Weizhen Zhang, Yue Yin and Hong Chen designed the study; Hong Chen and Lijun Sun performed most of the experiments and analyzed the data; Lu Feng, Xue Han, Yunhua Zhang, Wenbo Zhai and Zehe Zhang helped with the experiments; Hong Chen wrote the original draft; Weizhen Zhang reviewed and edited the manuscript; Yue Yin and Weizhen Zhang obtained funding and supervised the study. All authors have read and agreed to the published version of the manuscript.

Competing interests

The authors declare no competing interests.

Acknowledgments

This research was supported by grants from the National Natural Science Foundation of China (81930015, 81730020, 82070592 and 82270610), National Institutes of Health Grant R01DK112755 and 1R01DK129360.

Data availability

•All of the data supporting the findings of this study are included in the Article and Supplementary information. The Single-cell RNA sequencing data were uploaded to a

public database (PRJNA1031585). Source data are provided with this paper.

Abstract

Mechanism underlying the metabolic benefit of intermittent fasting remains largely unknown. Here, we reported that intermittent fasting promoted IL-22 production by type 3 innate lymphoid cells (ILC3s) and subsequent beigeing of subcutaneous white adipose tissue. Adoptive transfer of intestinal ILC3s increased beigeing of white adipose tissue in diet-induced-obese mice. Exogenous IL-22 significantly increased the beigeing of subcutaneous white adipose tissue. Deficiency of IL-22 receptor attenuated the beigeing induced by intermittent fasting. Single-cell sequencing of sorted intestinal immune cells revealed that intermittent fasting increased aryl hydrocarbon receptor signaling in ILC3s. Analysis of cell□cell ligand receptor interactions indicated that intermittent fasting may stimulate the interaction of ILC3s with dendritic cells (DCs) and macrophages. These results establish the role of intestinal ILC3s in beigeing of white adipose tissue, suggesting that ILC3/IL-22/IL-22R axis contributes to the metabolic benefit of intermittent fasting.

Key word:

ILC3s; IL-22; Beigeing of white adipose tissue; Intermittent fasting

Introduction

Obesity is defined as an epidemic metabolic disease characterized by excessive fat accumulation as the consequence of long-term energy surplus. Thus, therapeutic management of obesity has been focused on the restoration of energy balance, either by decreasing energy intake or increasing energy expenditure[1]. Among these strategies, intermittent fasting is becoming a popular dietary approach. All intermittent fasting schemes including alternate day fasting, 5:2 intermittent fasting and daily time-restricted feeding have shown the health benefits such as delaying aging[2-6], improving metabolism[7, 8], and enhancing cognition[9-11]. The mechanism underlying metabolic benefit of intermittent fasting remains largely unknown. Its metabolic benefit was initially attributed to limitation of energy intake. Recent studies have indicated an alternative mechanism involving beigeing of white adipose tissue, which accounts for the major plasticity of energy expenditure. Studies by Kim *et al.* have showed that intermittent fasting induces white adipose beigeing via stimulation of angiogenesis and macrophage M2 polarization[12]. On the other hand, studies by Li *et al.*[13] have indicated that alternate day fasting induces white adipose tissue beigeing by shaping the gut microbiota and elevating the fermentation products acetate and lactate. Although gut microbiota is closely related to immune response, it remains unclear whether intestinal immune cells contribute to the metabolic benefit of intermittent fasting.

Innate lymphoid cells (ILCs) are a group of natural immune cells lacking antigen-specific receptors expressed on T cells and B cells[14]. Based on developmental

trajectories, ILCs are divided into five groups: natural killer cells, type 1 ILCs, type 2 ILCs, type 3 ILCs (ILC3s) and lymphoid tissue-inducing cells[15]. Adipose-Resident type 1 ILCs can promote adipose tissue fibrosis and obesity-associated insulin resistance[16, 17] while type 2 ILCs promote beiging of white adipose tissue and limit obesity[18-20]. However, the contribution of ILC3s on adipocytes and obesity are less clear. ILC3s can produce interleukin-17 (IL-17) and interleukin-22 (IL-22) in response to extracellular bacteria and fungi[21]. ILC3s derived IL-22 can enhance the intestinal mucosal barrier function, reduce endotoxemia and inflammation, ameliorate insulin sensitivity[22, 23] and improve the metabolic disorder of polycystic ovary syndrome[24]. However, ILC3s are also reported to be involved in the induction of obesity[25], contributing to the metabolic disease [25-28]. Therefore, the role of ILC3s in metabolic disease seems complex and the role of ILC3s in intermittent fasting and beigeing of adipose tissue is not known.

Here, we showed that alternate day fasting promoted the secretion of IL-22 by ILC3s. Further, adoptive transfer of intestinal ILC3s increased thermogenesis in DIO mice. Exogenous IL-22 induced the beigeing of white adipose tissue. Deficiency of IL-22 receptor attenuated the beigeing of white adipose tissue induced by intermittent fasting. Our study demonstrates that intestinal ILC3-IL-22-IL-22R axis is actively involved in the regulation of adipose tissue beigeing. Our findings thus reveal a novel pathway in the dialog between the gut and adipose tissue.

Results

1. Intermittent fasting enhances IL-22 production by intestinal

ILC3s

To explore the effect of intermittent fasting on intestinal immune cells, we applied alternate-day fasting to mice fed normal chow diet (NCD-IF group) or high-fat diet (HFD-IF group) (Figure 1A). Intermittent fasting significantly reduced the body weight of mice fed HFD, while demonstrating no effect on food intake rate which was normalized to body weight (Figure 1—figure supplement 1A-B). Moreover, intermittent fasting decreased the respiratory quotient (RQ) on the fasting day while increased the energy consumption on the feeding day in mice fed HFD (Figure 1—figure supplement 1C-D), improved glucose and lipid metabolism in mice fed HFD (Figure 1—figure supplement 1E, F), and promoted white adipose tissue beigeing in mice fed NCD or HFD (Figure 1—figure supplement 2).

To explore whether gut immune system contributes to the effects of intermittent fasting on white adipose tissue beigeing, we examined levels of various cytokines in intestine. Notably, mRNA level of *Il22* in the NCD-IF group was significantly higher relevant to the control group (Figure 1B). Consistently, plasma concentration of IL-22 detected by ELISA was also increased (Figure 1C). These results suggest that intermittent fasting increases levels of IL-22 in the intestine and plasma. Since ILC3s are the main source of IL-22 in the small intestine[29-31], we detected the proportion of ILC3s in the lamina propria of small intestine using flow cytometry. In mice fed NCD, intermittent fasting significantly increased proportion of IL-22 positive ILC3s in the small intestine lamina propria (Figure 1D), while demonstrating no effect on the percentile of total ILC3s (Figure 1E). Interestingly, intermittent fasting did not

influence the secretion of IL-22 of T cells marked as Lineage^{+} Rorγ^{+} cells (Figure 1F). Besides, intermittent fasting didn't alter the levels of ILC3s and IL-22 in mouse adipose tissue (Figure 1G and Figure 1—figure supplement 3). Similar to NCD mice, intermittent fasting significantly increased mRNA levels of IL-22 in the intestine of HFD mice while didn't influence the secretion of IL-22 by T cells (Figure 1H-I). Furthermore, mice fed high-fat diet showed an obvious reduction in the plasma IL-22 (Figure 1J) and percentage of total and IL-22 positive ILC3s (Figure 1K). Further, the decrement of plasma IL-22 (Figure 1J) as well as IL-22 positive ILCs in intestine (Figure 1K) was attenuated by 30 days intermittent fasting.

In order to explain the chronological relationship between ILC3s secreting IL-22 and beigeing of white adipose tissue, the mice were exposed to one cycle of intermittent fasting for 2 days. At this time, the body weight of mice didn't change and beige adipocytes haven't been induced (Figure 1—figure supplement 4A-B). However, significant increase in proportion of IL-22 positive ILC3s was induced by intermittent fasting for two days whereas total percentile of ILC3s remained unalterd (Figure 1—figure supplement 4C). These results indicate that the beiging of white adipose tissue are subsequent to its effect on ILC3s secreting IL-22.

2. Intestinal ILC3s promote beigeing of white adipose tissue

Next, we examined whether adoptive transfer of intestinal ILC3s can increase beigeing of white adipose tissue in diet-induced obesity (DIO) mice. Intestinal ILC3s were isolated and purified from the small intestinal lamina propria of NCD mice (Figure 2—figure supplement 1A). These cells were defined as lineage^{-}

155 CD127^{+}KLRG1^{-}c-Kit^{+} cells (Figure 2—figure supplement 1B). As shown in Figure
156 2A, DIO mice transferred with ILC3s demonstrated a significant increment in the
157 proportion of small intestinal ILC3s. Previous researches report that intestinal ILC3s
158 specifically express gut homing receptors CCR7, CCR9, and α4β7[32-34], which may
159 explain transplantation of intestinal ILC3s can migrate mainly to the intestine instead
160 of adipose tissue. Plasma concentration of IL-22 also increased significantly relevant
161 to PBS control (Figure 2B). Relevant to PBS control, adoptive transfer of intestinal
162 ILC3s decreased body weight and weight of sWAT (Subcutaneous adipose tissue)
163 slightly, while had no impact on food intake and the liver weight (Figure 2—figure
164 supplement 1C-E). In addition, ILC3s from CD45.1 mouse intestinal lamina propria
165 lymphocytes were adoptively transferred into recipient mice, and CD45.1 positive
166 immune cells were significantly increased in intestine but not in adipose tissue in
167 mice transferred with ILC3s (Figure 2—figure supplement 1F), indicating the
168 feasibility of ILC3s adoptive transfer. Notably, DIO mice transferred with intestinal
169 ILC3s showed improved glucose tolerance (Figure 2C) and decreased levels of
170 random blood glucose (Figure 2D). Cold exposure experiment showed that DIO mice
171 transferred with intestinal ILC3s maintained significantly higher rectal temperatures
172 during a 6-h cold challenge (Figure 2E). Consistently, key thermogenic genes in
173 sWAT including *Ucp1* and *Cidea* were significantly increased (Figure 2F). Size of
174 adipocytes in the sWAT and eWAT was markedly reduced (Figure 2G-H).
175 Furthermore, differentiated SVF cells co-cultured with intestinal ILC3s in vitro
176 (Figure 2I) demonstrated a significant increment in the expression of *Ucp1* and

Pparg (Figure 2J), as well as a concurrent decrement in the size of lipid droplets (Figure 2K). On the other hand, co-culture with CD127$^-$ cells demonstrated no effect (Figure 2J-K). The in vitro experiment indicates the direct effect of ILC3s on adipocytes.

3. Exogenous IL-22 increases beigeing of white adipose tissue

The role of type 3 immunity in DIO and metabolic syndrome is complex. ILC3-derived IL-22 are beneficial in metabolic syndrome[22, 35] but can also contribute to metabolic disease[25-27]. In order to examine the role of promoting beigeing of white adipose tissue of IL-22 in the context of NCD and HFD mice, we intraperitoneally administrated IL-22 at the dose of 4 μg/kg body weight/every other day for 6 weeks into mice fed NCD or HFD. Saline was used as control. Administration of IL-22 increased its plasma concentration in mice fed either NCD or HFD (Figure 3—figure supplement 1A). Exogenous IL-22 significantly increased oxygen consumption, carbon dioxide production and energy expenditure in mice fed either NCD or HFD (Figure 3A-F). Respiratory quotient (RQ) was significantly reduced in mice fed NCD at dark and mice fed HFD at light (Figure 3G-H). No significant difference was observed for animal activity (Figure 3—figure supplement 1B). In addition, exogenous IL-22 significantly improved glucose tolerance in mice fed HFD (Figure 4A). Interestingly, body weight and food intake were not altered (Figure 3—figure supplement 1C-D), indicating that the metabolic benefit of IL-22 is not dependent on food intake. Consistent with previous research, IL-22 administration improves insulin sensitivity without change in body weight[36]. In addition, IL-22 can increase Akt

phosphorylation in muscle, liver and adipose tissues, leading to improvement in insulin sensitivity[22].

We next explored the effect of exogenous IL-22 on thermogenesis induced by 4°C cold exposure. Exogenous IL-22 rendered mice fed HFD resistant to core temperature drop induced by cold exposure (Figure 4B). Relevant to the pale yellow color in the control animals, subcutaneous fat of obese mice treated with exogenous IL-22 appeared dark yellowish (Figure 4C). The mRNA levels of thermogenic genes such as *Ucp1* were significantly increased by IL-22 (Figure 4D). Adipocyte size of subcutaneous adipose tissue and epididymal adipose tissue was significantly reduced in the animals treated with IL-22 (Figure 4E-4F). These observations suggest that intraperitoneal injection of IL-22 promotes the beigeing of white adipose tissue in mice.

To determine whether IL-22 can directly act on adipocytes to promote their beigeing, adipose tissue SVF was isolated and induced for beige differentiation. Il22ra1 mainly expressed on mature adipocytes (Figure 4—figure supplement 1A). IL-22 at the dose of 100 ng/mL was continuously administered during beige differentiation. IL-22 significantly increased SVF beige differentiation evidenced by cell morphology, increment in mRNA levels of genes relevant to thermogenesis, including *Ucp1* and *Cidea*, and protein level of UCP1(Figure 4G-I). IL-22 did not alter the levels of genes related to adipogenesis (Figure 4—figure supplement 1B). As expected, IL-22 increased the phosphorylation of STAT3 and MAPK (Figure4I, Figure 4—figure supplement 1C), which can increase the expression of thermogenic

genes[37, 38]. These results suggest that IL-22 can directly stimulate beigeing of white adipose tissue.

4. IL-22R knock-out blocks beigeing induced by intermittent fasting

To explore whether IL-22R mediates the effect of intermittent fasting on the beigeing of white adipose tissue, IL-22R knockout (IL-22RKO) mice and wild-type (WT) littermates were subjected to alternate-day fasting diet for 30 days. Rectal temperature of WT-IF and IL-22RKO-IF mice was monitored during two consecutive days of intermittent fasting. On the fasting day, the rectal temperature of IL-22RKO-IF mice was significantly lower than that of WT-IF mice at 16:00 time point (Figure 5A). On the feeding day, the rectal temperature of IL-22RKO-IF mice was lower at three time points: 8:00, 12:00 and 20:00 (Figure 5B). These results indicate that IL-22RKO attenuates the thermogenesis induced by intermittent fasting. Knock-out of IL-22R demonstrated no effect on the glucose tolerance and insulin sensitivity in mice fed NCD (Figure 5C-D). However, the weight of subcutaneous adipose tissue in IL-22RKO-IF mice increased significantly (Figure 5E). mRNA levels of the thermogenic gene *Ucp1* decreased substantially, whereas *Fabp4* increased (Figure 5F). Furthermore, knockout of IL-22R significantly attenuated the increment of multilocular lipid droplets and the decrement of adipocyte size in the subcutaneous fat induced by intermittent fasting (Figure 5G-H), indicating a reduction in beigeing.

To further explore whether IL-22R mediates the effect of ILC3s on beigeing of adipocytes, intestinal ILC3s isolated from intermittent fasting mice were co-cultured

with beige adipocytes from subcutaneous SVF of WT or IL-22RKO mice (Figure 5I-J). Co-culture with ILC3s significantly increased the mRNA levels of thermogenic genes in beige adipocytes derived from WT mice, while demonstrating no effect on beige adipocytes derived from IL-22RKO mice (Figure 5K). These observations indicate that IL-22R mediates the effect of intestinal ILC3s on beigeing of white adipocytes.

5. Profiling of intestinal immune cells in mice fed NCD, HFD or HFD-IF

To explore the mechanism by which intermittent fasting promotes the secretion of IL-22 by ILC3s, live $CD45^+$ Lineage (CD3, CD5, B220, CD19, Gr1)$^-$ cells isolated from the siLP of mice fed NCD, HFD or HFD-IF were subjected for single-cell sequencing (Figure 6—figure supplement 1A). Following quality controls, we analyzed 7455, 4803, 5954 single cells for the NCD, HFD and HFD-IF groups using Seurat-V3.1, respectively. Based on singleR, we identified twenty-five distinct clusters of immune cells (Figure 6A and Figure 6—figure supplement 1B), including ILC1s (Cluster 7 and cluster 16), ILC2s (Cluster 2, cluster 12, cluster 13, and cluster 14), ILC3s (cluster 3 and cluster 5), dendritic cells (Cluster 1, cluster 4, cluster 9, cluster 10, cluster 11, cluster 17, cluster 18, and cluster 21), eosinophils (Cluster 0 and cluster 6), B cells (Cluster 8 and cluster 24), macrophages (Cluster 15, cluster 20, and cluster 23), NKT cells (Cluster 22) and mast cells (Cluster 19). As expected, ILC3s expressed high RNA levels of Il7r (CD127), Rorc, and IL-22 (Figure 6B, C and Figure 6—figure supplement 1C-D). ILC3s contain two distinct cell types with highly

similar expression profiles: NCR^+ and NCR^-. These ILC3s were distinguished in our analysis as Cluster 5 and Cluster 3 respectively. NCR^- ILC3s (cluster 3) were CCR6 positive and contained lymphoid tissue inducer (LTi) cells (Figure 6B). Interestingly, NCR^- ILC3s were characterized by high levels of vasoactive intestinal peptide receptor 2 (Vipr2) (Figure 6C), which is critical for the migration and function of ILC3s[29, 39, 40]. The heatmap of cellular composition showed the differences in cell number and percentage among NCD, HFD and HFD IF mice (Figure 6—figure supplement 2A). The change in ILC3 number was consistent with the flow cytometry results. The percentage of IL-22^+ cells in NCR^+ ILC3s was significantly increased by IF in mice fed HFD (Figure 6—figure supplement 2B). Moreover, GSEA revealed that HFD-induced decrement of cytokine□cytokine receptor interaction, in which IL-22 is included, was reversed by IF (Figure 6—figure supplement 2C). Besides, Neuroactive ligand-receptor interaction, in which vipr2 is included, was up-regulated in HFD-IF (Figure 6—figure supplement 2D). The mRNA levels of *Vipr2* had a tendency to increase in in sorted ILC3s from the small intestine of HFD IF mice compared with that of HFD mice (Figure 6—figure supplement 2E). Further, gene difference analysis revealed that HFD-induced increase of Zmat4 was significantly attenuated by IF (Figure 6D, Figure 6—figure supplement 2F-G).

Further, the expression level of Hsp90ab1 in both NCR^- ILC3s and NCR^+ was significantly increased by IF in mice fed HFD (Figure 6D, Supplementary 10H). Transcription factor analysis using the JASPAR database and TFBS Tools revealed that the expression of *Hsp90ab1* may be regulated by aryl hydrocarbon receptor

(AHR) (Figure 6D). AHR is located in the Hsp90:XAP2:p23:Src chaperone protein complex in the cytoplasm without stimulation. Upon binding with the ligand, AhR translocates to the nucleus and heterodimerizes with AhR nuclear translocator (ARNT) to control the transcription of target genes, including AhR repressor (*Ahrr*), *Cyp1a1*, *Cyp1b1* and *Il22*[41]. Consistently, Gene Ontology analysis of the top 20 increased difference genes revealed that aryl hydrocarbon receptor signaling was one of the key pathways affected by intermittent fasting in HFD mice (Figure 6E-F). Furthermore, the AHR target genes, including *Il22*, *Ahrr*, *Cyp1a1*, *Cyp1b1*, increased significantly in ILC3s sorted from HFD-IF mice compared with HFD mice. These results indicates that intermittent fasting increases the production of IL-22 likely via activation of AhR.

6. IF ameliorates the impaired interaction between intestinal myeloid cells and ILC3s

Because dendritic cells (DCs) can influence the production of IL-22 by ILC3s, we next analyzed the change in DCs induced by intermittent fasting. IF significantly attenuated the increment of inflammatory factors, such as Ccl4, Ccl17 and Ccl22, of DCs in mice fed HFD (Figure 7A). Kyoto Encyclopedia of Genes and Genomes (KEGG) analysis of the top 20 differentially expressed genes in cluster 17 revealed that the increase of inflammation-related pathways induced by HFD was obviously attenuated by IF (Figure 7B-C). These observations indicate that intermittent fasting may ameliorate the inflammatory state of the intestine by decreasing the NOD-like receptor signaling pathway in DCs (Figure 7B-C).

We next analyzed the intestinal cellular communication networks using CellPhone

DB analysis based on homologous gene transformation on all immune cells acquired. CellPhone DB ligand□receptor analysis revealed hundreds of immune-to-immune interactions (Figure 7—figure supplement 1A). Connectome web analysis of siLP immune cells revealed strong interactions among $CD8^+$ dendritic cells (DC) (Cluster 4), $CD127^+$ ILC1s (Cluster 16), $DC8^-$ DC-1 (Cluster 9), Macrophages-1 (Cluster 15), $CD8^-$ DC-2 (Cluster 1), Macrophages-2 (Cluster 23), $CD8^-$ DC-3 (Cluster 10), $CD8^-$ DC-4 (Cluster 11), and $CD8^-$ DC-5 (Cluster 17). Notably, NCR^+ ILC3s strongly interacted with $CD8^+$ dendritic cells (DC) (Cluster 4), $CD127^+$ ILC1 s (Cluster 16), $DC8^-$ DC (Cluster 9), macrophages (Cluster 15), $CD8^-$ DC (Cluster 1), macrophages (Cluster 23), $CD8^-$ DC (Cluster 10), $CD8^-$ DC (Cluster 11), and $CD8^-$ DC (Cluster 17). ILC subsets, DCs and macrophages were in the central communication hubs of the healthy small intestine (Figure 7—figure supplement 1B-C). Analysis of highly expressed interactions uncovered various uncharacterized and validated signaling pathways implicated in intestine homeostasis in mice (Figure 7—figure supplement 1D). Analysis of the NCD mouse interactome suggests that macrophages (cluster 15) may interact with NCR^+ ILC3s through CD74_COPA, CD74_MIF, CD44_HBEGF, CD44_FGFR2, CCL4_SLC7A1, and IL1B_ADRB2. Similarly, DCs (cluster 9) may interact with NCR^+ILC3s through CD74_COPA, CD74_MIF, IL1B_ADRB2, CD44_HBEGF, and CD44_FGFR2. All these observations indicates that macrophages and DCs play critical roles in the recruitment and maintenance of ILC3s.

HFD significantly reduced the interaction between ILC subsets, DCs and macrophages in the small intestine (Figure 7D and Figure 7—figure supplement 1B).

This reduction was reversed by IF (Figure 7E and Figure 7—figure supplement 1B). Analysis of the interactomes in mice fed HFD suggested that IF significantly altered the interacting proteins (Figure 7F-G). To further test this observation, we sorted macrophages and ILC3s from HFD and HFD-IF mice (Figure 7—figure supplement 2A). As shown in supplementary Figure 10B-C, *Ccl4* and *Cd74* increased significantly in macrophages, while the receptors expressed on ILC3s remained largely unchanged (Figure 7—figure supplement 2B-C). Together, these data suggest that IF may promote the production of IL-22 from ILC3s by altering the interactome in intestinal myeloid cells and ILC3s.

Discussion

Our present study demonstrates that intestinal ILC3s are critical for the beigeing of white adipose tissue induced by intermittent fasting. This conclusion is supported by following observations. Firstly, intermittent fasting stimulates the secretion of IL-22 by intestinal ILC3s in either lean mice fed normal chow diet, obese mice fed high-fat diet mice, or mice with metabolic dysfunction induced by HFCD diet. Secondly, a comprehensive set of in vivo and in vitro experiments shows that intermittent fasting promotes adipose tissue beigeing through the intestinal ILC3-IL-22-IL-22R axis.

The role of ILC3s in metabolism remains largely unknown. Our studies provide evidence supporting the metabolic benefit of intestinal ILC3s in intermittent fasting. Adoptive transfer of intestinal ILC3s isolated from lean mice was sufficient to improve the metabolic dysfunctions in DIO mice, including increase of white adipose tissue beigeing and glucose tolerance. Interestingly, adoptive transfer of ILC3s

significantly increased their number only in intestine. Further, alternate day fasting did not alter the ILC3s in adipose tissue. These observations indicate that ILC3s in intestine rather than in adipose tissue account for the metabolic benefit. In addition to directly promoting the beigeing of white adipose tissue through IL-22, intestinal ILC3s may enhance the intestinal mucosal barrier[42], reducing serum LPS and peptidoglycan, thus reducing the inhibitory effect of LPS and peptidoglycan on the beigeing of white adipose tissue[43]. O'Sullivan et al.[16] have reported that ILC3s are negligible in white adipose tissue of either lean or obese mice. Similarly, Sasaki *et al*.[25] have demonstrated that transplanting bone marrow cells from Rag2$^{-/-}$ mice (lack of T cells, B cells) into Il2rg$^{-/-}$ Rag2$^{-/-}$ mice (lack of T cells, B cells, ILC cells) could not increase the number of ILC3s in the adipose tissue of recipient mice. However, it is worth of noting that ILC3s have been detected in adipose tissue by other report. Using the marker Lineage^{-}KLRG1^{-}Il-7rα^{+}Thy-1^{+}, ILC3s cells have been reported to account for approximately 20% of lineage^{-}KLRG1^{-}Il-7rα^{+} cells in adipose tissue. In our study, we also detected ILC3s defined as CD127^{+}Lin^{-}RORγt^{+} in adipose tissue. These ILC3s accounted for approximately 10% of CD127^{+}Lin^{-} cells. ILC3s have also been shown to be present in human adipose tissue[44]. Importantly, the proportion and density of ILC3s in white adipose tissue of people with obesity increase relevant to healthy people, and positively correlate with BMI in obese patients. Thus, the existence and function of ILC3s in mouse and human adipose tissue deserve further investigation.

Communication between intestine and metabolic organs is currently under active

investigation. Our studies identify ILC3s-IL-22-IL-22R as a novel pathway medicating the crosstalk between intestine and adipose tissue. Evidence supporting this conclusion are five folds. (1) Intermittent fasting reverses the reduction of intestinal ILC3s and IL-22 in DIO mice. (2) Adoptive transfer of intestinal ILC3s enhances beigeing of white adipose tissue. (3) Co-culture of intestinal ILC3s with SVF cells increases their differentiation into beige cells. (4) Exogenous IL-22 mimics the effect of intermittent fasting on beigeing of white adipose tissue. (5) Deficiency of IL-22R blocks the IF-induced beigeing of white adipose tissue. In lines with our observation, a series of recent studies have suggested that cytokines can act directly on adipocytes to regulate thermogenesis. For example, γδ T cells regulate heat production by secreting IL-17[45]. Deficiency of IL-10 increases energy consumption and renders mice resistant to diet-induced obesity[34]. IL-27-IL-27Rα signaling promotes thermogenesis, prevents diet-induced obesity, and improves insulin resistance[46]. IL-33 induces the beigeing of white adipose tissue by activating ILC2s[18]. Our studies extend the effect of cytokines on thermogenesis to IL-22. IL-22 promotes heat production, renders mice resistant to reduction of body temperature induced by cold exposure, and reduces obesity induced by high-fat diet. Together with previous report showing that IL-22 increases the lipolysis of adipocytes, our studies suggest that IL-22 can directly act on adipocytes to alter the adipose tissue homeostasis. IL-22 activates IL-22 receptor, which then regulates the expression of downstream inflammatory factors, tissue repair molecules, chemokines, antimicrobial peptides and other molecules via Jak-1 and Tyk-2 dependent phosphorylation of

STAT3. Our studies suggest that IL-22 may promote the expression of downstream thermogenic genes in adipose tissue through IL-22R. Deficiency of IL-22R blocks the up-regulation of thermogenic genes induced by intermittent fasting. SVF cells lacking IL-22R demonstrate no response to the up-regulation of thermogenic genes induced by intestinal ILC3. Thus, our results provide novel evidence supporting the concept that intestinal ILC3s modulate beigeing of adipose tissue via IL-22-IL-22R pathway.

The physiological mechanism underlying the secretion of IL-22 by ILC3s remains largely unknown. Our studies reveal the distinct secretion pattern of IL-22 induced by intermittent fasting. Consistently, previous studies have shown that secretion of IL-22 by ILC3s changes between active and quiescent periods throughout the day which is regulated by the cycle patterns of food intake[47]. These suggest that secretion of IL-22 by ILC3s is altered by feeding rhythm. It is currently unclear how feeding influences the physiological function of ILC3s. Previous studies indicate a mechanism involving neuropeptide vasoactive intestinal peptide (VIP), which is able to stimulate the secretion of IL-22 by ILC3s[29]. Consistently, our single cell RNAseq data also showedthat VIP receptor 2 (VIPR2) is highly expressed in intestinal ILC3s and intermittent fasting activates VIPR2 signaling pathway. Since release of VIP is stimulated by food intake, these observations indicate that VIP-VIPR signaling may coordinate with food intake to drive the production of IL-22. However, conflicting result exists. Studies by Talbot *et al* have shown that VIP inhibits ILC3 secretion of IL-22[39]. Reasons accounting for this difference remains unknown but may be context dependent. Alternatively, we found that intermittent fasting may promote ILC3s

secreting IL-22 though activating AhR signaling. In addition, feeding may decrease the levels of antimicrobial peptides secreted by epithelial cells, while increasing the expression of lipid-binding proteins[39]. Moreover, segmented filamentous bacteria may account for the effect of feeding on the secretion of IL-22 by intestinal ILC3s by periodically attaching to the epithelial surface[47]. These alterations may substantially influence the immune networks in intestine, leading to subsequent change in the secretion of IL-22 by ILC3s. In support of this concept, our single cell RNAseq analysis shows a significant change in the intestinal immune cell network involving dendritic cells, macrophages and ILC3s. Further examination should focus on dissecting the novel molecular mechanism by which intestinal dendritic cells and macrophages interact with ILC3s and its consequence on the IL-22 production.

In conclusion, our studies suggest that intermittent fasting can promote the secretion of IL-22 by intestinal ILC3s. IL-22 promotes beigeing of white adipose tissue through IL-22R. Intestinal ILC3s thus may serve as a potential target for the intervention of metabolic disorders.

Materials and Methods

Key Resources Table				
Reagent type (species) or resource	**Designation**	**Source or reference**	**Identifiers**	**Additional information**

antibody	eBioscience™ Fixable Viability Dye eFluor™ 606	Invitrogen	Cat# 65-0866-14	FACS (1:400)
antibody	PerCP/Cy5.5 anti-mouse CD45(30-F11)	BioLegend	Cat# 103131	FACS (1:400)
antibody	FITC anti-mouse CD3ε(RA3-6B2)	BioLegend	Cat# 103205	FACS (1:400)
antibody	FITC anti-mouse/human CD45R/B220(RA3-6B2)	BioLegend	Cat# 103205	FACS (1:400)
antibody	FITC anti-mouse Ly-6G/Ly-6C(Gr-1)(RB6-8C5)	BioLegend	Cat# 108405	FACS (1:400)
antibody	FITC anti-mouse CD19(6D5)	BioLegend	Cat# 115506	FACS (1:400)
antibody	FITC anti-mouse CD5(53-7.3)	BioLegend	Cat# 100605	FACS (1:400)
antibody	BV421 anti-mouse CD127(IL-7Rα)(A7R34)	BioLegend	Cat# 135023	FACS (1:400)
antibody	PE/Cyanine 7 anti-mouse CD90.2(30-H12)	BioLegend	Cat# 105325	FACS (1:400)

antibody	PE/Cyanine 7 anti-mouse CD45.1	BioLegend	Cat# 110729	FACS (1:400)
antibody	PE anti-mouse RORγt(Q31-378)	BD Pharmingen	Cat# 562607	FACS (1:400)
antibody	Alexa Fluor 647 anti-mouse IL-22(Poly5164)	BioLegend	Cat# 516406	FACS (1:400)
antibody	BV605 anti-mouse/human KLRG1(MAFA)(2F1/KLRG1)	BioLegend	Cat# 138419	FACS (1:400)
antibody	PE anti-mouse CD117(c-kit) (2B8)	BioLegend	Cat# 105807	FACS (1:400)
antibody	Rb polyclonal antibody to UCP1	abcam	Cat# ab10983	WB (1:1000)
antibody	Phospho-Stat3 (Tyr705) Rabbit mAb	Cell signaling technology	Cat# #9145	WB (1:1000)
antibody	Stat3 (124H6) Mouse mAb	Cell signaling technology	Cat# #9139	WB (1:1000)
antibody	Phospho-p38 MAPK (Thr180/Tyr182) (D3F9) XP® Rabbit mAb	Cell signaling technology	Cat# #4511	WB (1:1000)
antibody	p38 MAPK (D13E1) XP® Rabbit mAb	Cell signaling technology	Cat# #8690	WB (1:1000)
antibody	Rb polyclonal antibody to UCP1	abcam	Cat# ab10983	WB (1:1000)
commercial assay or kit	eBioscience™	Invitrogen	Cat# 00-8333-56	

	Fixation/Perm Diluent			

1. Animals

Four-week-old male C57BL/6 and CD45.1 mice were obtained from Charles River Laboratories (Peking, China). IL-22 receptor knockout mice (IL-22R KO mice, KO-00115) were purchased from BRL Medicine Inc. Mice were handled in accordance with the Guide for the Care and Use of Laboratory Animals prepared by the National Academy of Sciences and published by the National Institutes of Health (NIH publication 86-23, revised 1985). Mice were housed in standard rodent cages and maintained in a regulated environment (21-24°C, humidity at 40-70%, 12:12 h light : dark cycle with lights on at 8:00 AM). A normal chow diet (D12450H; Research Diets) and water were available ad libitum. Obese mice (DIO) were induced with a high-fat diet (60% fat, D12492; Research Diets) for 12 weeks. Eight-week-old C57BL/6 mice received intraperitoneal injection of saline control or IL-22 (R&D, 582-ML) at a dose of 4 μg/kg/day every other day for 6 weeks. All experimental procedures were approved by the Animal Care and Use Committee of Peking University (permit: LA2017099).

2. Cell preparation

For isolation of small intestine lamina propria cells, small intestines from euthanized mice were emptied of the contents, excised of Peyer's patches, opened longitudinally and cut into 1 cm pieces. The intraepithelial lymphocytes (IELs) were dissociated from the intestine fragments by first shaking the fragments for 20 min at

37°C in PBS containing 0.3% BSA, 5 mM EDTA and 1 mM dithiothreitol. Vortex the fragments three times with PBS containing 2 mM EDTA. To isolate lamina propria cells, the remaining fragments were minced and digested at 37°C for 50 min in RPMI 1640 medium containing 0.04 mg/mL collagenase (Sigma), 0.1 mg/mL deoxyribonuclease (DNase) I (Roche), and 0.5 mg/mL dispase. The digestion suspension was then filtered through a 40 μm cell strainer and centrifuged at 540 g for 6 min. Cell pellets were resuspended in PBS containing 2% FBS for further analysis.

3. Flow cytometry

Single-cell suspensions were preincubated with anti-CD16/32 (clone 2.4G2) for 10 min to block the surface Fc receptors. Then, cell-surface molecules were stained with different antibody combinations for 30 min in cell staining buffer. Dead cells were excluded with Fixable Viability Dye eFluor^{TM} 606 (Invitrogen). For intracellular transcription factor staining, the cells were fixed and permeabilized with a Foxp3 staining buffer set (eBioscience) according to the manufacturer's protocol. Transcription factor staining usually lasted for more than 4 hours at 4°C. The gate strategy for ILC3s was live lingeage (CD3, CD5, CD19, B220 and Gr-1)$^{-}$ CD127^{+}RORγt^{+}. For intracellular cytokine staining, the digested cells were first incubated in RPMI 1640 with 10% FBS and 10 ng/ml recombinant murine IL-7 (PeproTech), and stimulated with 50 ng/ml phorbol 12-myristate 13-acetate, 750 ng/ml ionomycin for 3 h and added with 2 μM monensin for the last 2.5 h.

Flow cytometry analyses were performed on an LSR Fortessa (BD Biosciences). The flow cytometry data were analyzed with FlowJo software (Tree Star). The

antibody used in this study are listed in Supplementary Table 1.

4. ILC3s sorting, transfer and co-culture experiment

For ILC3s transfer experiment, co-culture experiment and single-cell RNA-Seq, ILCs were collected by FACS. Small intestine lamina propria cells from male C57BL/6J mice were prepared and stained with surface molecules for 30 min at 4□ followed by sorting on a FACS Aria III cell sorter (BD Biosciences). A gating strategy of live Lineage^{-}CD127^{+}KLRG1^{-}c-Kit^{+} was used to sort the ILC3s.

Purification checks were performed after each sort. The cells were suspended in phosphate buffered saline（PBS）and then intravenously injected into HFD mice (200 μL PBS/mouse). ILC3s were sorted from 20 WT NCD mice, and sorting for the adoptive transfer was performed six times within 4 weeks from the first injection. The total number of ILC3 injected into HFD mice was 2.4×10^{5} cells/mouse/experiment. Mice were placed on an HFD for 16 weeks before ILC3s were transferred. In addition, to confirm that these cells indeed originate from NCD mice, we transferred ILC3s from CD45.1 mice to WT mice and detected the CD45.1 positive cells in recipient mice.

5. Single-cell RNA-Seq

Single cells were captured via the GemCode Single Cell Platform using the GemCode Gel Bead, Chip and Library Kits (10X Genomics) according to the manufacturer’s protocol. Briefly, flow-sorted cells were suspended in PBS containing 0.4% BSA and loaded at 6,000 cells per channel. The cells were then partitioned into a GemCode instrument, where individual cells were lysed and mixed with beads

carrying unique barcodes in individual oil droplets. The products were subjected to reverse transcription, emulsion breaking, cDNA amplification, shearing, 5′ adaptor and sample index attachment. Libraries were sequenced on a HiSeq 2500 (Illumina).

6. Isolation of stromal vascular fraction cells (SVF) and induction of beigeing

Isolation of SVF and induction of beigeing were performed as reported[48]. Briefly, subcutaneous white adipose tissue (sWAT) from male C57BL/6 mice was digested with 1 mg/mL type 2 collagenase (Sigma Aldrich) at 37°C for 40 minutes with shaking. Digestion was terminated by complete DMEM/F12 medium containing 10% fetal bovine serum (FBS), 100 units/mL penicillin and 100 units/mL streptomycin (Invitrogen, CA, USA). The cell suspension was centrifuged at 700×g for 10 minutes to separate floating adipocytes from the SVF pellets. The pellets containing the SVF cells were resuspended in complete medium and filtered using a 70 μm diameter filter. The cell suspension was then centrifuged at 700×g for 10 minutes. Cell pellets were resuspended and mixed well and then plated on dishes in complete medium. Cells were grown to 95% confluence in complete medium and then differentiated into beige or white adipocytes as previously described[49]. Briefly, for induction to beige adipocytes, cells were cultured for 2 days with induction medium supplemented with 5 μg/mL insulin, 1 nmol/L T3, 1 μmol/L rosiglitazone, 125 μmol/L indomethacin, 0.5 mmol/L isobutylmethylxanthine (IBMX) and 5 μmol/L dexamethasone. Cells were then cultured in maintenance medium supplemented with 5 μg/ml insulin, 1 nmol/L T3 and 1 μmol/L rosiglitazone for 4 days. Fresh media were replaced every 2 days.

7. Co-culture experiments

To determine the direct effect of ILC3s on beige adipocytes differentiation, SVF were co-cultured with ILC3s using a transwell system (0.4 μm pore size, BD Biosciences). In brief, SVF isolated from adipose tissue were grown in the bottom chamber of the transwell insert in a 12-well plate and induced into beige adipocytes, while sorted ILC3s were seeded in the upper chamber. SVFs cultured alone and SVF cells co-cultured with $CD127^-$ cells were used as controls. After co-culture for 72 h, beige adipocytes in the lower chamber were collected for further detection.

8. RNA isolation and qPCR analysis

RNA was extracted from cells or adipose tissue using RNATrip (Applied Gene, Beijing, China) and reverse-transcribed into cDNAs with Hifair™ III 1st Strand cDNA Synthesis SuperMix (Yeasen). SYBR Green-based quantitative real-time PCR was performed using the Agilent Aria Mx real-time PCR system. The primer sequences used in this study are listed in Supplementary File 1.

9. Western blot analysis

Differentiated SVF cells and sWAT were homogenized using RIPA lysis buffer. Proteins were separated by 10% sodium dodecyl sulfate–polyacrylamide gel electrophoresis and then transferred onto a nitrocellulose (NC) membrane. Membranes were incubated in 5% fat-free milk for 1 hour at room temperature and then incubated with primary antibodies overnight at 4°C. The reaction was detected with IRDye-conjugated secondary antibody and visualized using the Odyssey infrared imaging system (LI-COR Biosciences).

10. Histological studies

Paraffin-embedded sWAT sections were stained with hematoxylin-eosin (H&E). Images were scanned using a NanoZoomer-SQ (Hamamatsu).

11. Oil red O staining

Cells were washed with PBS for three times, and then fixed with 4% paraformaldehyde for 30 minutes. Next, the cells were stained with oil red O for 60 minutes, and washed with PBS for 5 minutes. Cells were then stained with hematoxylin for 5 seconds and washed with PBS. The dyed cells were photographed under the microscope (Leica, Germany).

12. Enzyme-linked immunosorbent assay

Levels of IL-22 were measured by double-antibody sandwich enzyme-linked immunosorbent assays (ELISAs) (M2200; R&D Systems). Briefly, 100 μL of Assay Diluent were added to each well. 50 uL of blood samples and standards were added and incubated at room temperature for 2 hours. After washing, conjugates were added and incubated for 2 hours. After washing, the substrate solution was added and incubated for 30 minutes and washed. And stop solution were added finally. Optical density (OD) values were measured using a microplate reader (Bio-Rad, Hercules, CA, USA).

13. OGTT and ITT

Oral Glucose tolerance tests (OGTT) and insulin tolerance tests (ITT) were performed after 16 or 6 hours of fasting, respectively. Mice were given with 3 g/kg glucose by gavage or injected intraperitoneally with 0.75 U/kg insulin. Blood samples

were collected from the tail vain at 0, 15, 30, 60, 90 and 120 min after glucose or insulin treatment. Blood glucose levels were measured using a glucometer (Roche, Basel, CH).

14. Cold exposure

Mice were placed in a 4°C cold room for 6 hours. The rectal temperature was measured every hour during the cold challenge with a rectal probe (Braintree Scientific, Braintree, MA).

15. Statistical analysis

Data were analyzed by GraphPad Prism software v.8.0 and presented as the mean ±s.e.m. The Shapiro–Wilk normality test was used to determine the normal distribution of samples. Unpaired Student's *t* test (normal distribution) or Mann–Whitney U-tests (non-normal distribution) was used to analyze data between two groups and one-way ANOVA followed by Bonferroni's multiple-comparisons test (normal distribution) or Kruskal–Wallis test (non-normal distribution) was used for three or more groups. The sample sizes were determined by power analysis using StatMate v.2.0. No data were excluded during the data analysis.

References

[1] Liu B, Du Y, Wu Y, Snetselaar L G, Wallace R B, Bao W. Trends in obesity and adiposity measures by race or ethnicity among adults in the united states 2011-18: Population based study. Bmj. 2021, 372: n365

[2] Colman R J, Anderson R M, Johnson S C, Kastman E K, Kosmatka K J, Beasley T M, Allison D B, Cruzen C, Simmons H A, Kemnitz J W, Weindruch R. Caloric restriction delays disease onset and mortality in rhesus monkeys. Science (New York, N.Y.). 2009, 325(5937): 201-204

[3] Mattison J A, Roth G S, Beasley T M, Tilmont E M, Handy A M, Herbert R L, Longo D L, Allison D B, Young J E, Bryant M, Barnard D, Ward W F, Qi W, Ingram D K, de Cabo R. Impact of caloric restriction on health and survival in rhesus monkeys from the nia study. Nature. 2012, 489(7415): 318-321

[4] Mattison J A, Colman R J, Beasley T M, Allison D B, Kemnitz J W, Roth G S, Ingram D K, Weindruch R, de Cabo R, Anderson R M. Caloric restriction improves health and survival of rhesus monkeys. Nature Communications. 2017, 8: 14063

[5] Ulgherait M, Midoun A M, Park S J, Gatto J A, Tener S J, Siewert J, Klickstein N, Canman J C, Ja W W, Shirasu-Hiza M. Circadian autophagy drives iTRF-mediated longevity. Nature. 2021, 598(7880): 353-358

[6] Stekovic S, Hofer S J, Tripolt N, Aon M A, Royer P, Pein L, Stadler J T, Pendl T, Prietl B, Url J, Schroeder S, Tadic J, Eisenberg T, Magnes C, Stumpe M, Zuegner E, Bordag N, Riedl R, Schmidt A, Kolesnik E, Verheyen N, Springer A, Madl T, Sinner F, de Cabo R, Kroemer G, Obermayer-Pietsch B, Dengjel J, Sourij H, Pieber T R, Madeo F. Alternate day fasting improves physiological and molecular markers of aging in healthy, non-obese humans. Cell Metabolism. 2019, 30(3): 878-881

[7] de Cabo R, Mattson M P. Effects of intermittent fasting on health, aging, and disease. New England Journal of Medicine. 2019, 381(26): 2541-2551

[8] Hepler C, Weidemann B J, Waldeck N J, Marcheva B, Cedernaes J, Thorne A K, Kobayashi Y, Nozawa R, Newman M V, Gao P, Shao M, Ramsey K M, Gupta R K, Bass J. Time-restricted feeding mitigates obesity through adipocyte thermogenesis. Science. 2022, 378(6617): 276-284

[9] Mattson M P, Moehl K, Ghena N, Schmaedick M, Cheng A. Intermittent metabolic switching, neuroplasticity and brain health. Nature Reviews. Neuroscience. 2018, 19(2): 63-80

[10] Liu Y, Cheng A, Li Y-J, Yang Y, Kishimoto Y, Zhang S, Wang Y, Wan R, Raefsky S M, Lu D, Saito T, Saido T, Zhu J, Wu L-J, Mattson M P. Sirt3 mediates hippocampal synaptic adaptations to intermittent fasting and ameliorates deficits in app mutant mice. Nature Communications. 2019, 10(1): 1886

[11] Mattson M P, Arumugam T V. Hallmarks of brain aging: Adaptive and pathological modification by metabolic states. Cell Metabolism. 2018, 27(6): 1176-1199

[12] Kim K-H, Kim Y H, Son J E, Lee J H, Kim S, Choe M S, Moon J H, Zhong J, Fu K, Lenglin F, Yoo J-A, Bilan P J, Klip A, Nagy A, Kim J-R, Park J G, Hussein S M, Doh K-O, Hui C-C, Sung H-K. Intermittent fasting promotes adipose thermogenesis and metabolic homeostasis via VEGF-mediated alternative activation of macrophage. Cell Research. 2017, 27(11): 1309-1326

[13] Li G, Xie C, Lu S, Nichols R G, Tian Y, Li L, Patel D, Ma Y, Brocker C N, Yan T, Krausz K W, Xiang R, Gavrilova O, Patterson A D, Gonzalez F J. Intermittent fasting promotes white adipose browning and decreases obesity by shaping the gut microbiota. Cell Metabolism. 2017, 26(4): 672-685.e674

[14] Gasteiger G, Fan X, Dikiy S, Lee S Y, Rudensky A Y. Tissue residency of innate lymphoid cells in lymphoid and nonlymphoid organs. Science (New York, N.Y.). 2015, 350(6263): 981-985

[15] Vivier E, Artis D, Colonna M, Diefenbach A, Di Santo J P, Eberl G, Koyasu S, Locksley R M, McKenzie A N J, Mebius R E, Powrie F, Spits H. Innate lymphoid cells: 10 years on. Cell. 2018, 174(5): 1054-1066

[16] O'Sullivan T E, Rapp M, Fan X, Weizman O-E, Bhardwaj P, Adams N M, Walzer T, Dannenberg A J, Sun J C. Adipose-resident group 1 innate lymphoid cells promote obesity-associated insulin resistance. Immunity. 2016, 45(2): 428-441

[17] Wang H, Shen L, Sun X, Liu F, Feng W, Jiang C, Chu X, Ye X, Jiang C, Wang Y, Zhang P, Zang M, Zhu D, Bi Y. Adipose group 1 innate lymphoid cells promote adipose tissue fibrosis and diabetes in obesity. Nat Commun. 2019, 10(1): 3254

[18] Brestoff J R, Kim B S, Saenz S A, Stine R R, Monticelli L A, Sonnenberg G F, Thome J J, Farber D L, Lutfy K, Seale P, Artis D. Group 2 innate lymphoid cells promote beiging of white adipose tissue and limit obesity. Nature. 2015, 519(7542): 242-246

[19] Lee M W, Odegaard J I, Mukundan L, Qiu Y, Molofsky A B, Nussbaum J C, Yun K, Locksley R M, Chawla A. Activated type 2 innate lymphoid cells regulate beige fat biogenesis. Cell. 2015, 160(1-2): 74-87

[20] Wang L, Luo Y, Luo L, Wu D, Ding X, Zheng H, Wu H, Liu B, Yang X, Silva F, Wang C, Zhang X, Zheng X, Chen J, Brigman J, Mandell M, Zhou Z, Liu F, Yang X O, Liu M. Adiponectin restrains ILC2 activation by ampk-mediated

feedback inhibition of IL-33 signaling. J Exp Med. 2021, 218(2):

[21] Sanos S L, Bui V L, Mortha A, Oberle K, Heners C, Johner C, Diefenbach A. Rorgammat and commensal microflora are required for the differentiation of mucosal interleukin 22-producing NKp46^{+} cells. Nature Immunology. 2009, 10(1): 83-91

[22] Wang X, Ota N, Manzanillo P, Kates L, Zavala-Solorio J, Eidenschenk C, Zhang J, Lesch J, Lee W P, Ross J, Diehl L, van Bruggen N, Kolumam G, Ouyang W. Interleukin-22 alleviates metabolic disorders and restores mucosal immunity in diabetes. Nature. 2014, 514(7521): 237-241

[23] Hasnain S Z, Borg D J, Harcourt B E, Tong H, Sheng Y H, Ng C P, Das I, Wang R, Chen A C H, Loudovaris T, Kay T W, Thomas H E, Whitehead J P, Forbes J M, Prins J B, McGuckin M A. Glycemic control in diabetes is restored by therapeutic manipulation of cytokines that regulate beta cell stress. Nature Medicine. 2014, 20(12): 1417-1426

[24] Qi X, Yun C, Sun L, Xia J, Wu Q, Wang Y, Wang L, Zhang Y, Liang X, Wang L, Gonzalez F J, Patterson A D, Liu H, Mu L, Zhou Z, Zhao Y, Li R, Liu P, Zhong C, Pang Y, Jiang C, Qiao J. Gut microbiota–bile acid–interleukin-22 axis orchestrates polycystic ovary syndrome. Nature Medicine. 2019, 25(8): 1225-1233

[25] Sasaki T, Moro K, Kubota T, Kubota N, Kato T, Ohno H, Nakae S, Saito H, Koyasu S. Innate lymphoid cells in the induction of obesity. Cell Reports. 2019, 28(1): 202-217.e207

[26] Upadhyay V, Poroyko V, Kim T J, Devkota S, Fu S, Liu D, Tumanov A V, Koroleva E P, Deng L, Nagler C, Chang E B, Tang H, Fu Y X. Lymphotoxin regulates commensal responses to enable diet-induced obesity. Nat Immunol. 2012, 13(10): 947-953

[27] Wang Y, Kuang Z, Yu X, Ruhn K A, Kubo M, Hooper L V. The intestinal microbiota regulates body composition through nfil3 and the circadian clock. Science. 2017, 357(6354): 912-916

[28] Kawano Y, Edwards M, Huang Y, Bilate A M, Araujo L P, Tanoue T, Atarashi K, Ladinsky M S, Reiner S L, Wang H H, Mucida D, Honda K, Ivanov, II. Microbiota imbalance induced by dietary sugar disrupts immune-mediated protection from metabolic syndrome. Cell. 2022, 185(19): 3501-3519.e3520

[29] Seillet C, Luong K, Tellier J, Jacquelot N, Shen R D, Hickey P, Wimmer V C, Whitehead L, Rogers K, Smyth G K, Garnham A L, Ritchie M E, Belz G T. The neuropeptide vip confers anticipatory mucosal immunity by regulating ILC3 activity. Nature Immunology. 2020, 21(2): 168-177

[30] Victor A R, Nalin A P, Dong W, McClory S, Wei M, Mao C, Kladney R D, Youssef Y, Chan W K, Briercheck E L, Hughes T, Scoville S D, Pitarresi J R, Chen C, Manz S, Wu L C, Zhang J, Ostrowski M C, Freud A G, Leone G W, Caligiuri M A, Yu J. Il-18 drives ILC3 proliferation and promotes IL-22 production via nf-κb. J Immunol. 2017, 199(7): 2333-2342

[31] Gronke K, Hernández P P, Zimmermann J, Klose C S N, Kofoed-Branzk M, Guendel F, Witkowski M, Tizian C, Amann L, Schumacher F, Glatt H, Triantafyllopoulou A, Diefenbach A. Interleukin-22 protects intestinal stem cells against genotoxic stress. Nature. 2019, 566(7743): 249-253

[32] Kim M H, Taparowsky E J, Kim C H. Retinoic acid differentially regulates the migration of innate lymphoid cell subsets to the gut. Immunity. 2015, 43(1): 107-119

[33] Mackley E C, Houston S, Marriott C L, Halford E E, Lucas B, Cerovic V, Filbey K J, Maizels R M, Hepworth M R, Sonnenberg G F, Milling S, Withers D R. Ccr7-dependent trafficking of rorγ□ ilcs creates a unique microenvironment within mucosal draining lymph nodes. Nat Commun. 2015, 6: 5862

[34] Yu H B, Yang H, Allaire J M, Ma C, Graef F A, Mortha A, Liang Q, Bosman E S, Reid G S, Waschek J A, Osborne L C, Sokol H, Vallance B A, Jacobson K. Vasoactive intestinal peptide promotes host defense against enteric pathogens by modulating the recruitment of group 3 innate lymphoid cells. Proc Natl Acad Sci U S A. 2021, 118(41):

[35] Zou J, Chassaing B, Singh V, Pellizzon M, Ricci M, Fythe M D, Kumar M V, Gewirtz A T. Fiber-mediated nourishment of gut microbiota protects against diet-induced obesity by restoring IL-22-mediated colonic health. Cell Host Microbe. 2018, 23(1): 41-53.e44

[36] Qi X, Yun C, Sun L, Xia J, Wu Q, Wang Y, Wang L, Zhang Y, Liang X, Wang L, Gonzalez F J, Patterson A D, Liu H, Mu L, Zhou Z, Zhao Y, Li R, Liu P, Zhong C, Pang Y, Jiang C, Qiao J. Gut microbiota-bile acid-interleukin-22 axis orchestrates

polycystic ovary syndrome. Nat Med. 2019, 25(8): 1225-1233

[37] Li H, Dong M, Liu W, Gao C, Jia Y, Zhang X, Xiao X, Liu Q, Lin H. Peripheral IL-6/stat3 signaling promotes beiging of white fat. Biochim Biophys Acta Mol Cell Res. 2021, 1868(10): 119080

[38] Zhang Y, Xie C, Wang H, Foss R M, Clare M, George E V, Li S, Katz A, Cheng H, Ding Y, Tang D, Reeves W H, Yang L J. Irisin exerts dual effects on browning and adipogenesis of human white adipocytes. Am J Physiol Endocrinol Metab. 2016, 311(2): E530-541

[39] Talbot J, Hahn P, Kroehling L, Nguyen H, Li D, Littman D R. Feeding-dependent vip neuron-ILC3 circuit regulates the intestinal barrier. Nature. 2020, 579(7800): 575-580

[40] Yu H B, Yang H, Allaire J M, Ma C, Graef F A, Mortha A, Liang Q, Bosman E S, Reid G S, Waschek J A, Osborne L C, Sokol H, Vallance B A, Jacobson K. Vasoactive intestinal peptide promotes host defense against enteric pathogens by modulating the recruitment of group 3 innate lymphoid cells. Proceedings of the National Academy of Sciences of the United States of America. 2021, 118(41): e2106634118

[41] Stockinger B, Di Meglio P, Gialitakis M, Duarte J H. The aryl hydrocarbon receptor: Multitasking in the immune system. Annu Rev Immunol. 2014, 32: 403-432

[42] Ibiza S, García-Cassani B, Ribeiro H, Carvalho T, Almeida L, Marques R, Misic A M, Bartow-McKenney C, Larson D M, Pavan W J, Eberl G, Grice E A, Veiga-Fernandes H. Glial-cell-derived neuroregulators control type 3 innate lymphoid cells and gut defence. Nature. 2016, 535(7612): 440-443

[43] Chen H, Sun L, Feng L, Mulholland M, Zhang W, Yin Y. Peptidoglycan inhibits beigeing of adipose tissue. Acta Pharm Sin B. 2022, 12(2): 990-993

[44] Hildreth A D, Ma F, Wong Y Y, Sun R, Pellegrini M, O'Sullivan T E. Single-cell sequencing of human white adipose tissue identifies new cell states in health and obesity. Nature Immunology. 2021, 22(5): 639-653

[45] Hu B, Jin C, Zeng X, Resch J M, Jedrychowski M P, Yang Z, Desai B N, Banks A S, Lowell B B, Mathis D, Spiegelman B M. γδ T cells and adipocyte il-17rc control fat innervation and thermogenesis. Nature. 2020, 578(7796): 610-614

[46] Wang Q, Li D, Cao G, Shi Q, Zhu J, Zhang M, Cheng H, Wen Q, Xu H, Zhu L, Zhang H, Perry R J, Spadaro O, Yang Y, He S, Chen Y, Wang B, Li G, Liu Z, Yang C, Wu X, Zhou L, Zhou Q, Ju Z, Lu H, Xin Y, Yang X, Wang C, Liu Y, Shulman G I, Dixit V D, Lu L, Yang H, Flavell R A, Yin Z. Il-27 signalling promotes adipocyte thermogenesis and energy expenditure. Nature. 2021, 600(7888): 314-318

[47] Brooks J F, Behrendt C L, Ruhn K A, Lee S, Raj P, Takahashi J S, Hooper L V. The microbiota coordinates diurnal rhythms in innate immunity with the circadian clock. Cell. 2021, 184(16): 4154–4167.e4112

[48] Aune U L, Ruiz L, Kajimura S. Isolation and differentiation of stromal vascular cells to beige/brite cells. J Vis Exp. 2013, (73): 50191

[49] Seale P, Conroe H M, Estall J, Kajimura S, Frontini A, Ishibashi J, Cohen P, Cinti S, Spiegelman B M. Prdm16 determines the thermogenic program of subcutaneous white adipose tissue in mice. The Journal of Clinical Investigation. 2011, 121(1): 96-105

Figure and Figure Legends

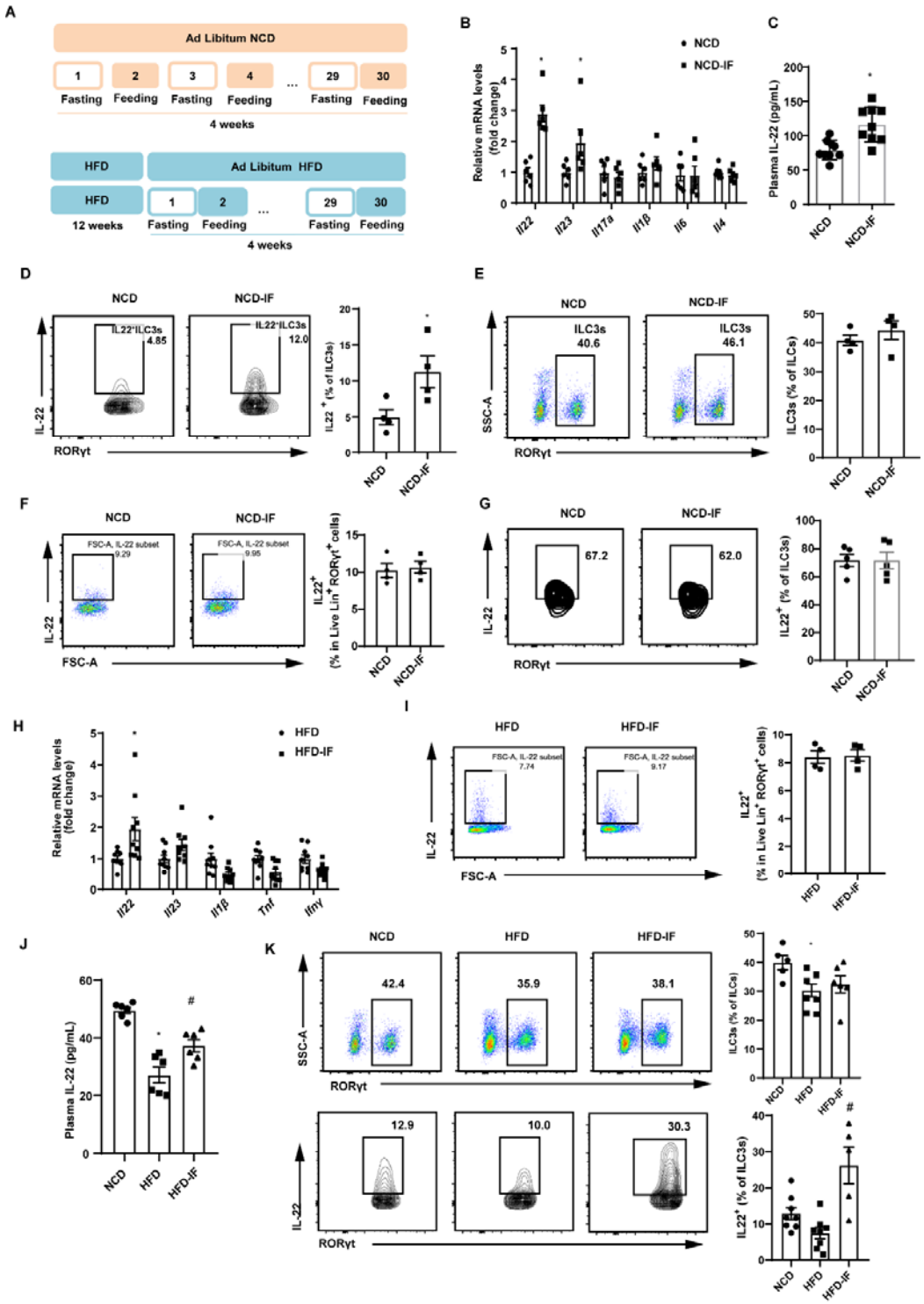

Figure 1. Intermittent fasting enhances IL-22 production by intestinal ILC3s.

A Schematic illustration of the alternate day fasting regimen. NCD, normal chow diet. HFD, high-fat diet. We applied alternate-day fasting to mice fed normal chow diet

(NCD-IF group) or high-fat diet (HFD-IF group). The control groups were at free access to NCD (NCD group) or HFD (HFD group). n = 9 for each group.

B mRNA expression levels of cytokine genes in the small intestine of NCD and NCD intermittent fasting (NCD-IF) mice. qPCR results were normalized to β-actin. n=6 for each group.

C Protein levels of IL-22 in plasma of NCD and NCD intermittent fasting (NCD-IF) mice. n=9 for each group.

D Flow cytometric analysis of IL-22^{+} cells in live CD127^{+} lineage^{-} RORγt^{+} ILC3s from the small intestine lamina propria (siLP) of NCD and NCD intermittent fasting (NCD-IF) mice. Four independent experiments were performed with similar results. n = 4.

E Flow cytometric analysis of RORγt^{+} ILC3s in live CD127^{+} lineage^{-} ILCs in the small intestine lamina propria of NCD and NCD intermittent fasting (NCD-IF) mice. n = 4.

F Flow cytometric analysis of IL-22^{+} cells in Live Lineage^{+} RORγt^{+} cells in the small intestine lamina propria of mice fed NCD with or without intermittent fasting. n = 4.

G Flow cytometric analysis of IL-22^{+} cells in CD90.2^{+} Lineage^{-} RORγt^{+} ILC3s from the SVF cells of sWAT in mice fed NCD with or without intermittent fasting. n= 5.

H mRNA expression levels of cytokine genes in the small intestine of mice fed HFD with or without intermittent fasting. qPCR results were normalized to β–actin. n= 9.

I Flow cytometric analysis of IL-22^{+} cells in Live Lineage^{+} RORγt^{+} cells in the small intestine lamina propria of mice fed HFD with or without intermittent fasting. n=4.

J Levels of IL-22 in plasma of NCD mice, HFD mice and HFD-IF mice. n=6.

K Flow cytometric analysis of RORγt^{+} ILC3s in live CD127^{+} lineage^{-} ILCs and flow cytometric analysis of IL-22^{+} cells in live CD127^{+} lineage^{-} RORγt^{+} ILC3s from the small intestine lamina propria of NCD mice, HFD mice and HFD-IF mice. n=5-8. * vs NCD, # vs HFD, $P < 0.05$.

All data represent the mean ± s.e.m. Statistical significance was determined by unpaired two-tailed Student's *t* test (A-I) or one-way ANOVA (J-K). NCD, normal chow diet. HFD, high-fat diet. NCD-IF, normal chow diet with intermittent fasting. HFD-IF, high-fat diet with intermittent fasting.

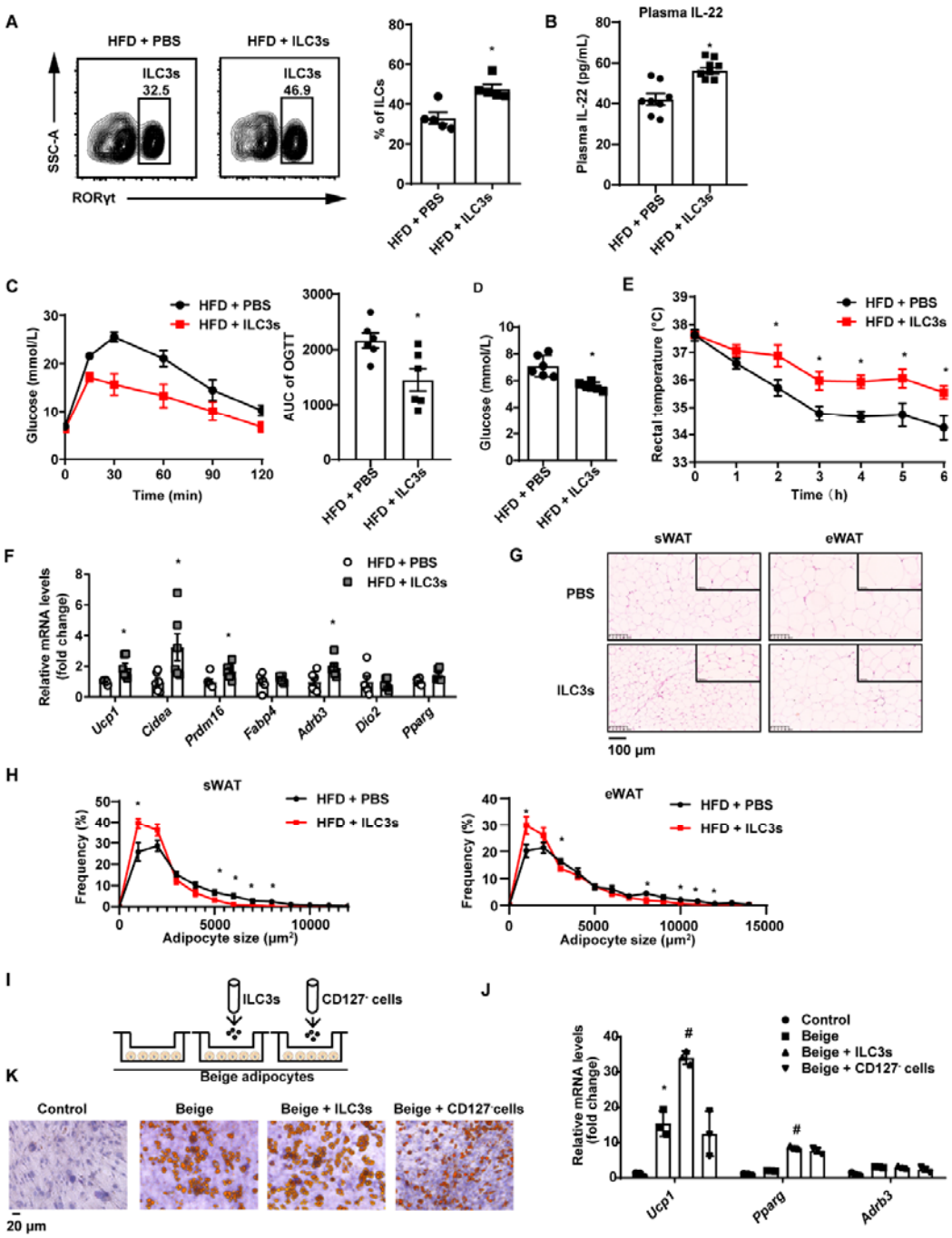

Figure 2. ILC3s promote beigeing of white adipose tissue.

6 weeks old male C57BL/6J SPF wild type mice were fed with HFD for 16 weeks and then injected with ILC3s (HFD + ILC3s group) or PBS (HFD + PBS group) intravenously six times in a month. n=8 for each group.

A. Flow cytometric analysis of RORγt^{+} ILC3s in live CD127^{+} lineage^{-} ILCs from the

siLP of mice transferred with PBS or ILC3s. The proportion of ILC3s in ILCs was shown in the histogram. n=5 for each group.

B. Levels of IL-22 in plasma. n=8 for each group.

C. Oral glucose tolerance test (OGTT) and area under the curve (AUC). n=6 mice/group.

D. Random blood glucose. n=6 mice/group.

E. Rectal temperature of HFD mice transferred with PBS or ILC3s during a 6 h cold challenge (4 °C). n=6 mice/group.

F. qPCR analysis of thermogenic genes in sWAT. n=6 mice/group.

G. Representative images of hematoxylin-and-eosin-stained sections of sWAT, eWAT and BAT from HFD mice transferred with ILC3s or control (n=5).

H. Distribution and average adipocyte size of sWAT and eWAT were shown (n=5).

I. Schematic depicting the coculture of ILC3s with SVF-derived beige adipocytes.

J. qPCR analysis of thermogenic genes in SVF-derived cells. * indicates $P<0.05$ vs Control, # denotes $P<0.05$vs Beige. n=3.

K. Oil red O staining of adipocytes after coculture with ILC3s or $CD127^-$ cells.

All data represent the means ± SEM. Statistical significance was determined by unpaired two-tailed Student's *t* test (A-H), one-way ANOVA(J).

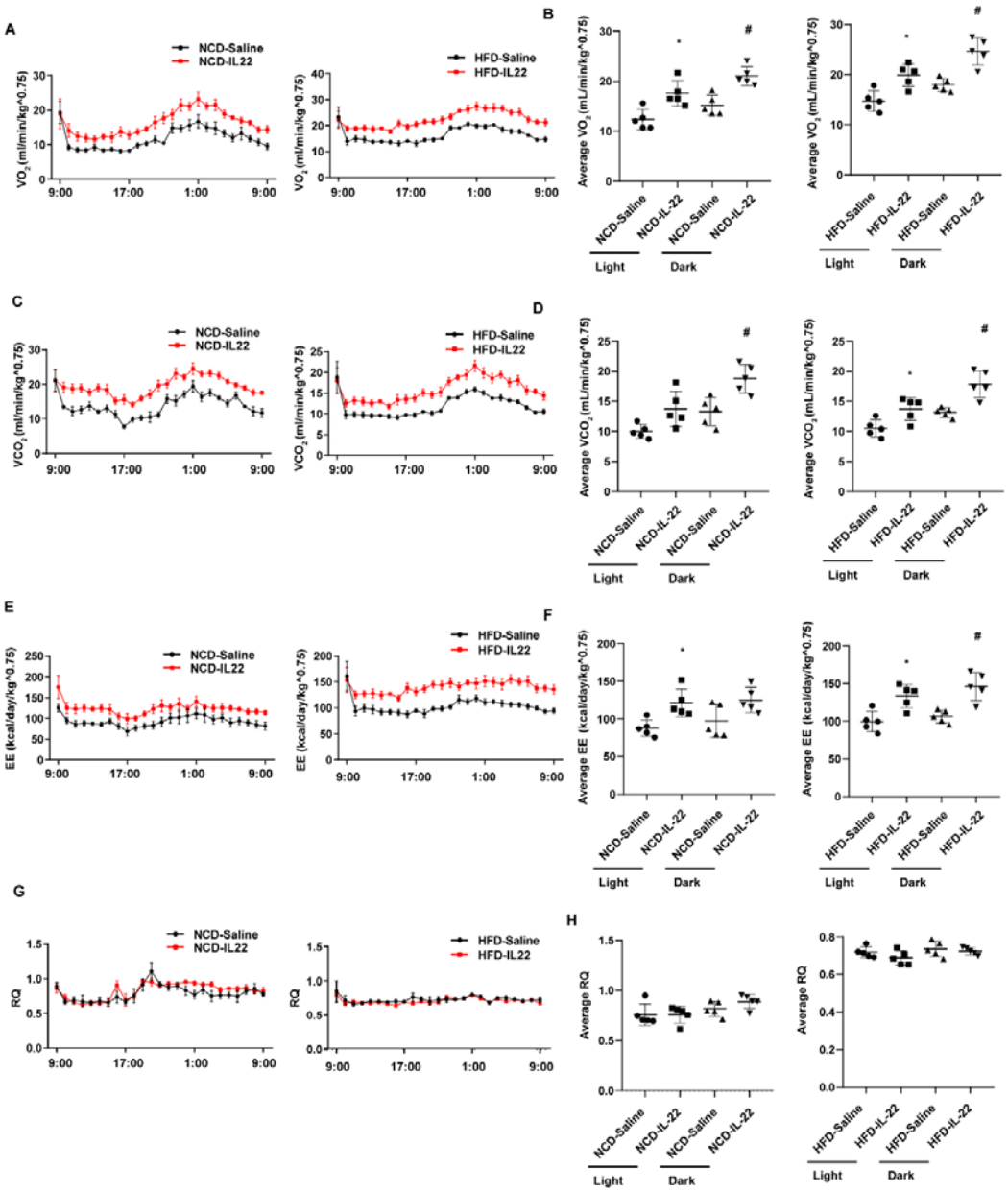

Figure3. IL-22 promotes energy expenditure.

6 weeks old male C57BL/6J SPF wild type mice were fed NCD or HFD for 12 weeks and then divided into four groups (NCD-Saline, NCD-IL-22, HFD-Saline, HFD-IL-22). Mice were intraperitoneally injected with 4 μg/kg IL-22 every other day for six weeks. The control groups were injected with saline.

A VO_2 of mice fed NCD or HFD.

B. Average VO_2 at light and dark respectively.

C. VCO_2 of mice fed NCD or HFD.

D. Average VCO_2 at light and dark respectively.

E. Energy expenditure of mice fed NCD or HFD.

F. Average energy expenditure at light and dark respectively.

G. Respiratory quotient (RQ) of mice fed NCD or HFD

H. Average respiratory quotient at light and dark respectively.

* indicates $P<0.05$ vs NCD-Saline or HFD-Saline at light. # indicates $P<0.05$ vs NCD-Saline or HFD-Saline at dark. n = 5. Statistical significance was determined by one-way ANOVA (B, D, F, H).

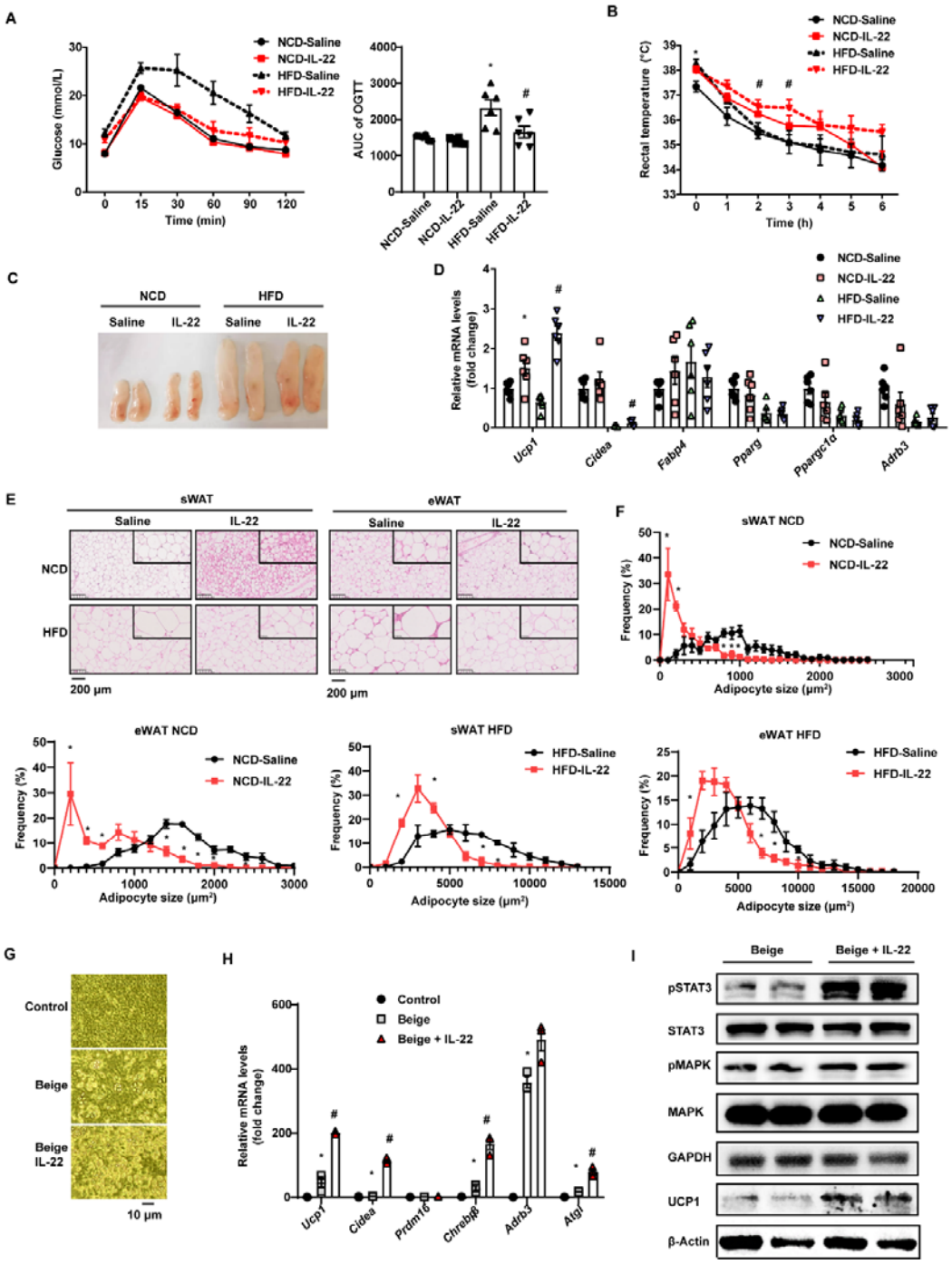

Figure 4. IL-22 promotes beigeing of white adipose tissue.

6 weeks old male C57BL/6J SPF wild type mice were fed NCD or HFD for 12 weeks and then divided into four groups (NCD-Saline, NCD-IL-22, HFD-Saline, HFD-IL-22). Mice were intraperitoneally injected with 4 μg/kg IL-22 every other day for 6

weeks. The saline group was injected with saline. n=6 mice/group.

A. Oral glucose tolerance test (OGTT) and area under the curve (AUC). n=6 mice/group. * indicates P<0.05 vs NCD-Saline; # denotes P<0.05 vs HFD-Saline.

B. Rectal temperature of mice during a 6 h cold challenge (4 °C). n=6. * indicates P<0.05 vs NCD-Saline; # denotes P<0.05 vs HFD-Saline.

C. Representative image of sWAT of the four groups, NCD-Saline, NCD-IL-22, HFD-Saline, HFD-IL-22.

D. qPCR analysis of thermogenic genes of sWAT. n=6 mice/group. * indicates P<0.05 vs NCD-Saline; # denotes P<0.05 vs HFD-Saline.

E. Representative images of hematoxylin-and-eosin-stained sections of sWAT and eWAT (n=5 for each group).

F. The distribution and average adipocyte size of sWAT and eWAT were determined by ImageJ.

G. Phase-contrast microscopic images of SVF cells and adipocytes.

H. qPCR analysis of thermogenic genes in SVF cells and beige adipocytes. n=3. # denotes P<0.05 vs Beige.

I. pSTAT3, STAT3, pMAPK, MAPK, GAPDH, UCP1, β-Actin protein expression in the beige adipocytes or beige adipocytes treated with IL-22 detected by Western blotting. GAPDH and β-Actin was used as the loading control.

All data represent the mean ± s.e.m. Statistical significance was determined by one-way ANOVA (A-D, H) or two-tailed Student's *t* test (F). sWAT, subcutaneous white adipose tissue; eWAT, epididymal white adipose tissue.

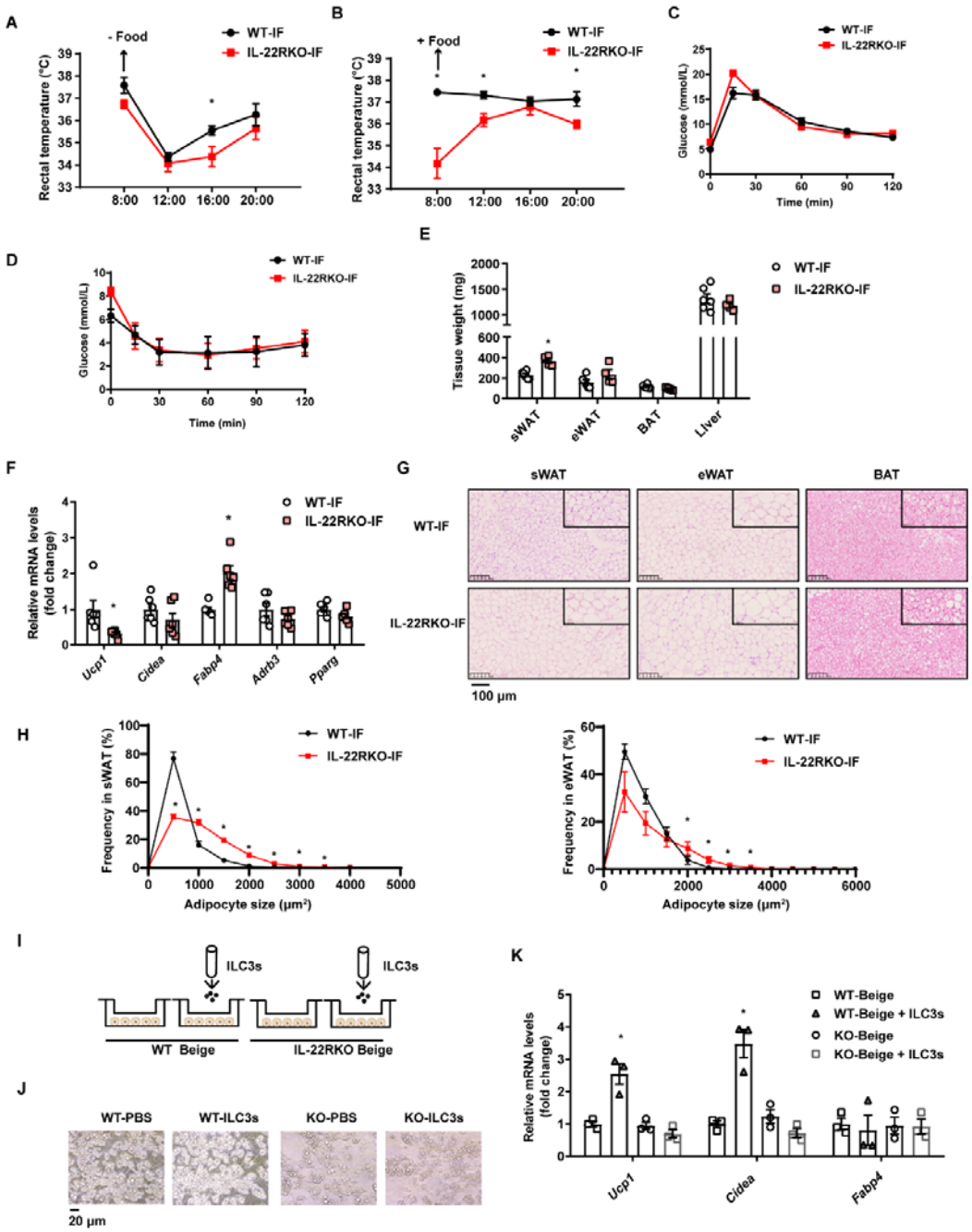

Figure 5. IL-22RKO blocks white adipose tissue beigeing induced by intermittent fasting.

8 weeks old IL-22RKO and wild type mice were subjected to alternate day fasting for 30 days. n =6 mice per group.

A. Rectal temperature of mice at room temperature during the fasting day. n=6 per

group.

B. Rectal temperature of mice at room temperature during the fed day. n=6 per group.

C. Oral glucose tolerance test (OGTT) of WT-IF mice and IL-22RKO-IF mice. n=6 per group.

D. Insulin tolerance test (ITT) of WT-IF mice and IL-22RKO-IF mice. n=6 per group.

E. Tissue weight of sWAT, eWAT, BAT, and liver from WT-IF and IL-22RKO-IF mice. n=6 mice/group.

F. qPCR analysis of thermogenic genes in sWAT from WT-IF and IL-22RKO-IF mice. n=6 mice/group.

G. Representative images of hematoxylin-and-eosin-stained sections of sWAT, eWAT and BAT (n=5 for each group).

H. The distribution and average adipocyte size of sWAT and eWAT were determined by ImageJ.

I. Schematic depicting the co-culture of ILC3s with SVF-induced beige adipocytes from WT or IL-22RKO mice. n=3. Experiments were repeated 3 times.

J. Phase contrast microscopy images of beige adipocytes differentiated from SVF cells cocultured with or without ILC3s. Shown are representatives from one experiment.

K. qPCR analysis of thermogenic genes in SVF-derived cells co-cultured with or without ILC3s. n=3.

All data represent the means ± SEM. Statistical significance was determined by unpaired two-tailed Student's *t* test (A-H) or one-way ANOVA (K).

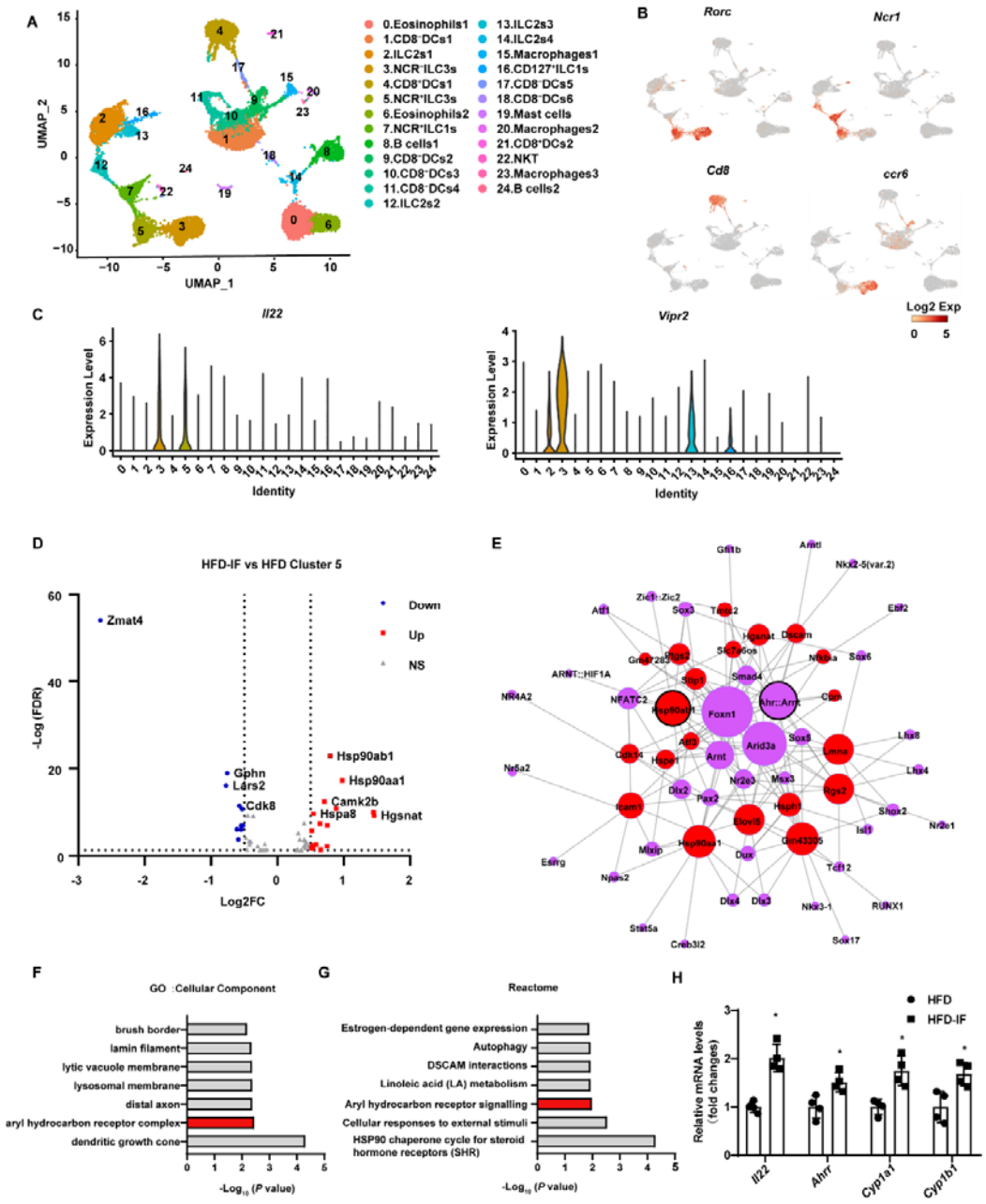

Figure 6. Profiling of intestinal immune cells derived from mice fed NCD, HFD and HFD-IF.

Live CD45+ Lineage -Cells sorted from mice fed normal chow diet (NCD group), high-fat diet (HFD- group), high-fat diet with alternate day fasting (HFD-IF group) were analyzed using single cell sequencing.

A. Cell subsets in the small intestine lamina propria $CD45^{+}$ $Lineage^{-}$ immune cell

atlas. Two-dimensional (2D) representation of cell profiles (dots) from the small intestine lamina propria, colored and numbered by cluster membership.

B-C. UMAP feature plots (B) and violin plots (C) showing RNA expression of cluster markers for the indicated cell populations. UMAP feature plots are based on the UMAP shown in Figure 6A.

D. The volcano plot of differentially expressed genes in Cluster 5 (NCR^+ ILC3s). The red dots represent upregulated genes in HFD-IF group compared with HFD group, while the blue dots represent downregulated genes in HFD-IF group compared with HFD group. Hsp90ab1 is one of the notably upregulated genes.

E. Transcription factor prediction using the Jaspar database and TFBS tools. Red dots represent differentially expressed genes, purple dots represent transcription factors, and larger nodes represent more nodes connected to them.

F. Gene ontology (GO) of the top 20 differentially expressed genes in Cluster 5. The cellular component up GO terms in HFD-IF group compared with HFD group.

G. The reactome up terms of Cluster 5 top 20 differential genes in HFD-IF group compared with HFD group.

H. qPCR analysis of AHR target genes in ILC3s sorted from HFD and HFD-IF mice. n=4. *, $P<0.05$, All data represent the means ± SEM. Statistical significance was determined by unpaired two-tailed Student's *t* test.

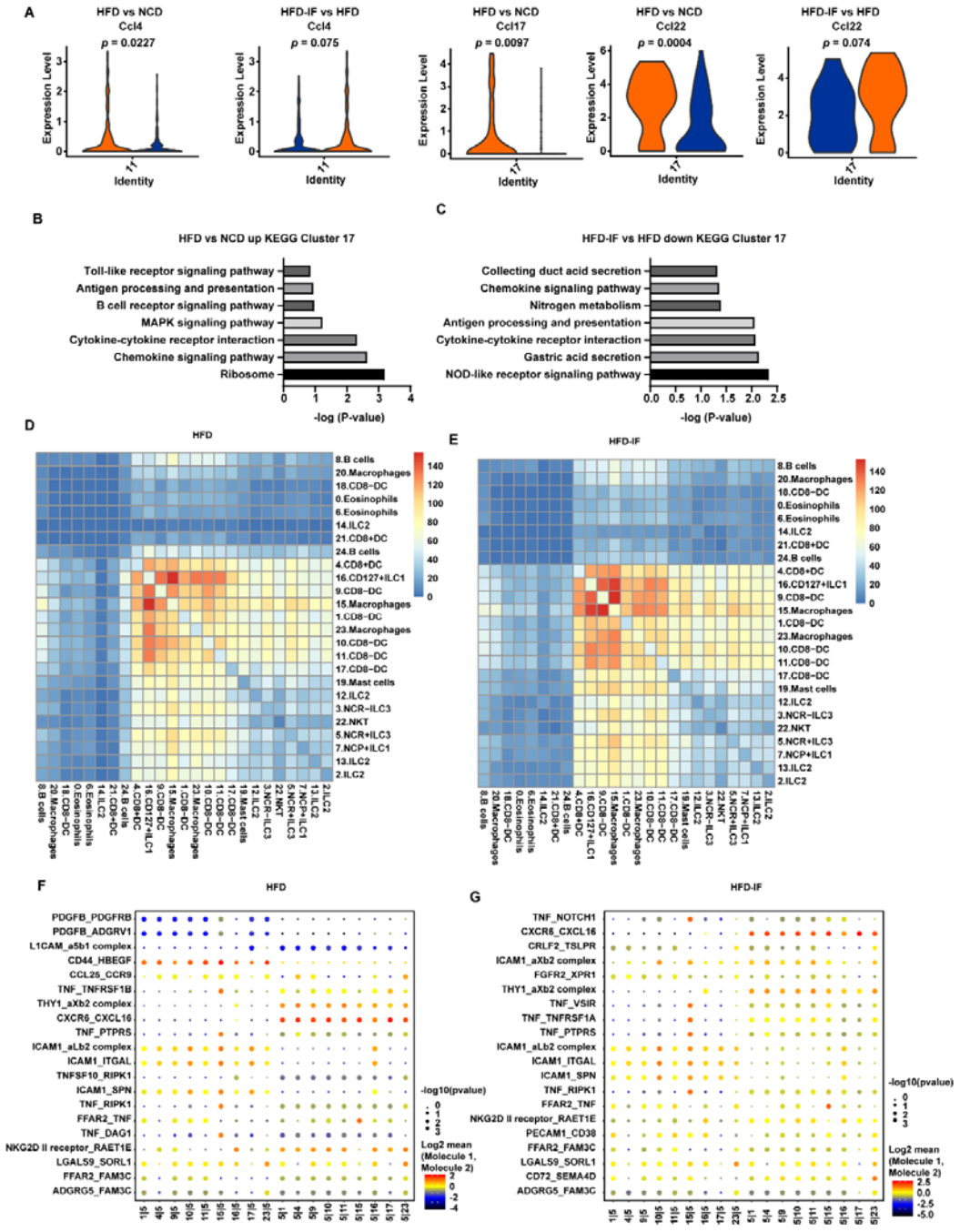

Figure 7. Interaction between myeloid cells and ILC3s.

A. Violin plots showing the RNA expression of chemokines in CD8$^-$DCs (cluster 11 and cluster 17).

B. KEGG enrichment in upregulated genes of CD8$^-$DCs of HFD group compared with NCD group (cluster 17).

C. KEGG enrichment of downregulated genes of $CD8^-$DCs of HFD-IF group compared with HFD group (cluster 17).

D. Heatmap showing the number of significant interactions identified between cell types in sorted siLP immune cells of HFD mice as determined by Cellphone DB. The color represents the number of interactions between cell types, a higher number of interactions (red) and a lower number of interactions (blue).

E. Heatmap showing the number of significant interactions identified between cell types in sorted siLP immune cells of HFD-IF mice as determined by Cellphone DB. The color represents the number of interactions between cell types: a higher number of interactions (red) and a lower number of interactions (blue).

F. Interaction pattern of the top 20 protein pairs and the top 20 cell types in sorted siLP immune cells of HFD group mice. The x-axis is the cell type interaction, and the y-axis is the protein interaction. The larger the point is, the smaller the p value. The color represents the average expression, and red to black indicates the level from high to low.

G. Interaction pattern of the top 20 protein pairs and the top 20 cell types in sorted siLP immune cells of HFD-IF mice. The x-axis is the cell type interaction, and the y-axis is the protein interaction. The larger the point is, the smaller the p value. The color represents the average expression, and red to black indicates the level from high to low.

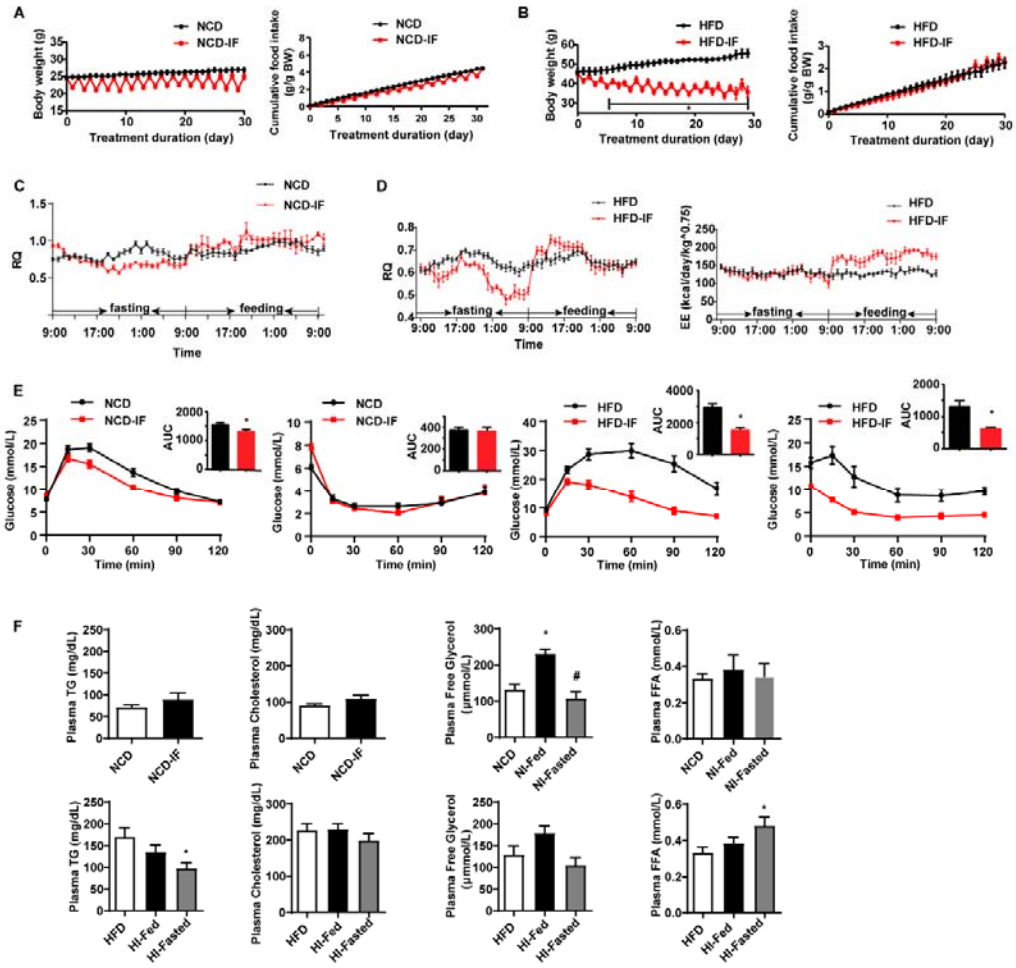

Figure 1—figure supplement 1 Intermittent fasting improves glucose metabolism and lipid metabolism.

A. Body weight and cumulative food intake normalized to body weight of mice fed NCD with or without intermittent fasting. n=9.

B. Body weight and cumulative food intake normalized to body weight of mice fed HFD with or without intermittent fasting. n=9.

C. Respiratory quotient (RQ) of mice fed NCD with or without intermittent fasting. n=5.

D. Respiratory quotient (RQ), energy expenditure (EE) of mice fed HFD with or

without intermittent fasting. n=5.

E. Oral glucose tolerance test (OGTT) and area under the curve (AUC). Insulin tolerance test (ITT) and area under the curve (AUC) of NCD, NCD-IF, HFD and HFD-IF mice. n=6 per group.

F. Levels of plasma triglycerides (TG), cholesterol, free glycerol and free fatty acids (FFA). n=6 mice/group.

All data represent the mean ± s.e.m. Statistical significance was determined by unpaired two-tailed Student's *t* test or one-way ANOVA.

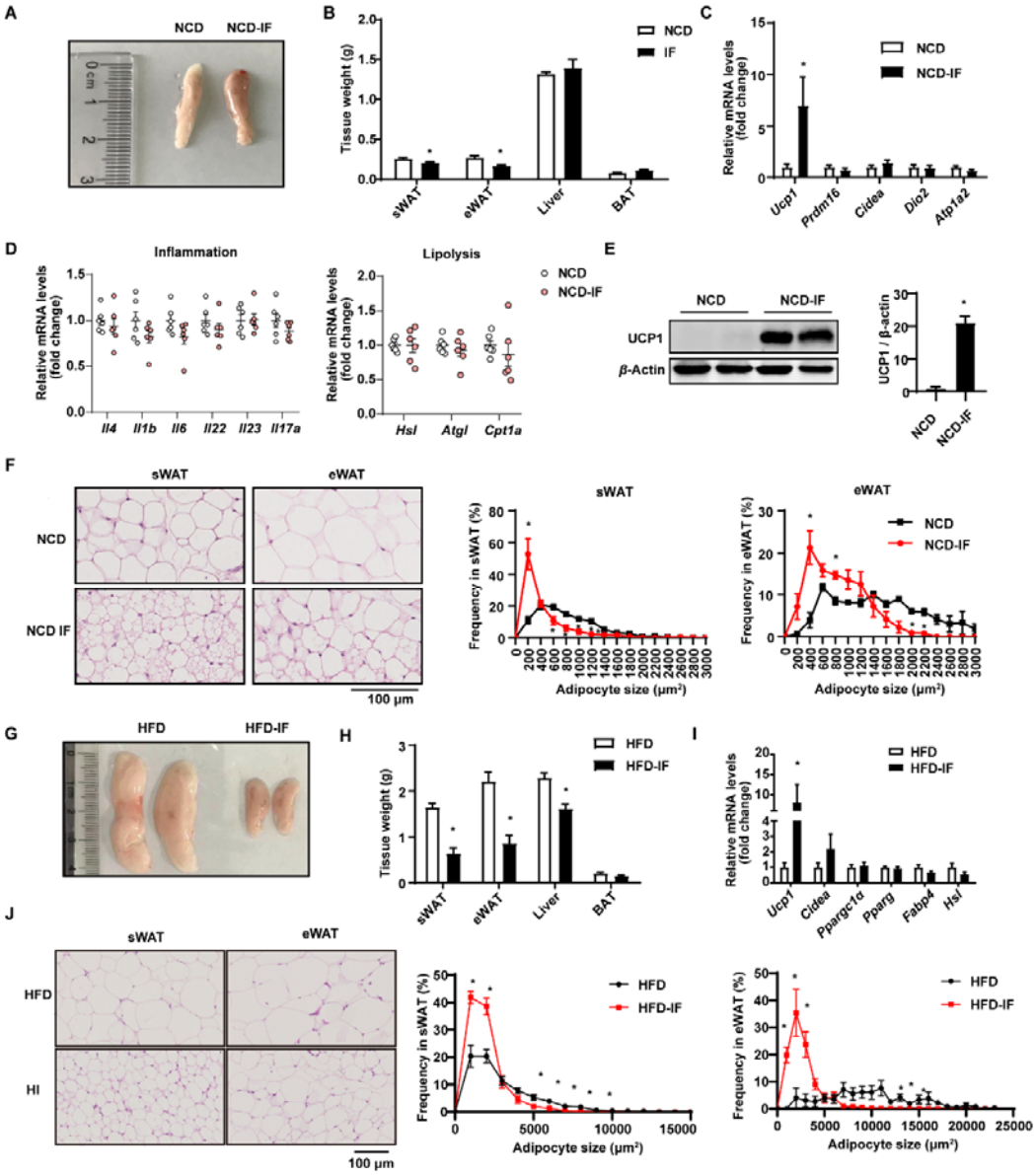

Figure 1—figure supplement 2 Intermittent fasting promotes white adipose tissue beigeing.

A. Representative image of sWAT from mice fed NCD with or without intermittent fasting.

B. Tissue weight of sWAT, eWAT, Liver, BAT, from NCD and NCD-IF mice. n=6.

C. qPCR analysis of thermogenic genes in sWAT from NCD and NCD-IF mice. n=6 mice/group.

D. qPCR analysis of inflammation and lipolysis genes in sWAT from NCD and NCD-IF mice. n=6 mice/group.

E. UCP1 protein expression in the sWAT of NCD and NCD IF mice detected by Western blotting. β-actin was used as the loading control. The relative protein signal intensity was quantified using ImageJ software.

F. H&E staining in sWAT and eWAT. Cell sizes were measured using ImageJ. n=5 per group. Scale bar: 100 μm.

G.Representative image for sWAT of HFD and HFD-IF mice. n=6.

H. Tissue weight of sWAT, BAT, Liver, eWAT from HFD and HFD-IF mice. n=6.

I. qPCR analysis of thermogenic genes in sWAT from HFD and HFD-IF mice. n=6 mice/group.

J. H&E staining in sWAT and eWAT from HFD and HFD-IF mice. Cell sizes were measured using ImageJ. n=5 per group. Scale bar: 100 μm.

All data represent the mean ± s.e.m. Statistical significance was determined by unpaired two-tailed Student's *t* test (B-E, H, I).

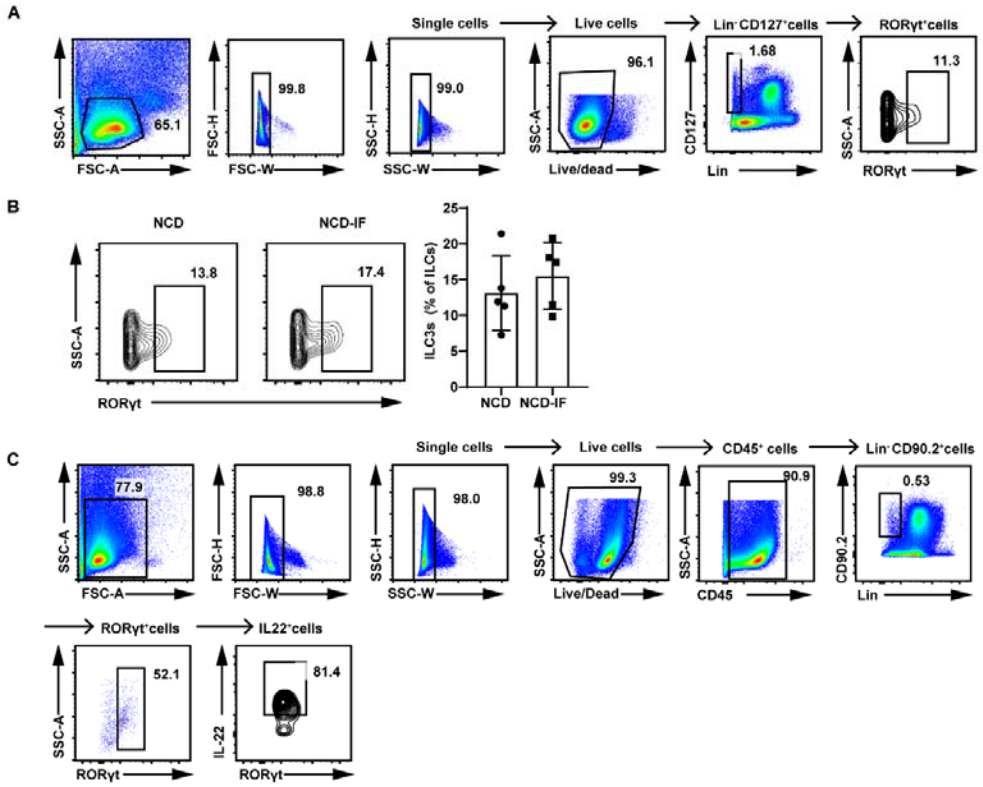

Figure 1—figure supplement 3 Intermittent fasting demonstrates no effect on the number of ILC3s in sWAT.

A. Gating strategy for flow cytometry analysis of live lineage^{-}CD127^{+}RORγt^{+}ILC3s in the SVF of sWAT.

B. Flow cytometric analysis of RORγt^{+} ILC3s in live CD127^{+} lineage^{-} ILCs from the sWAT of NCD mice, NCD-IF mice. n=5.

C. Gating strategy for flow cytometry analysis of IL-22^{+} cells in live CD45^{+}lineage^{-}CD90.2^{+}RORγt^{+}ILC3s in the SVF of sWAT.

All data represent the mean ± s.e.m. Statistical significance was determined by unpaired two-tailed Student's *t* test.

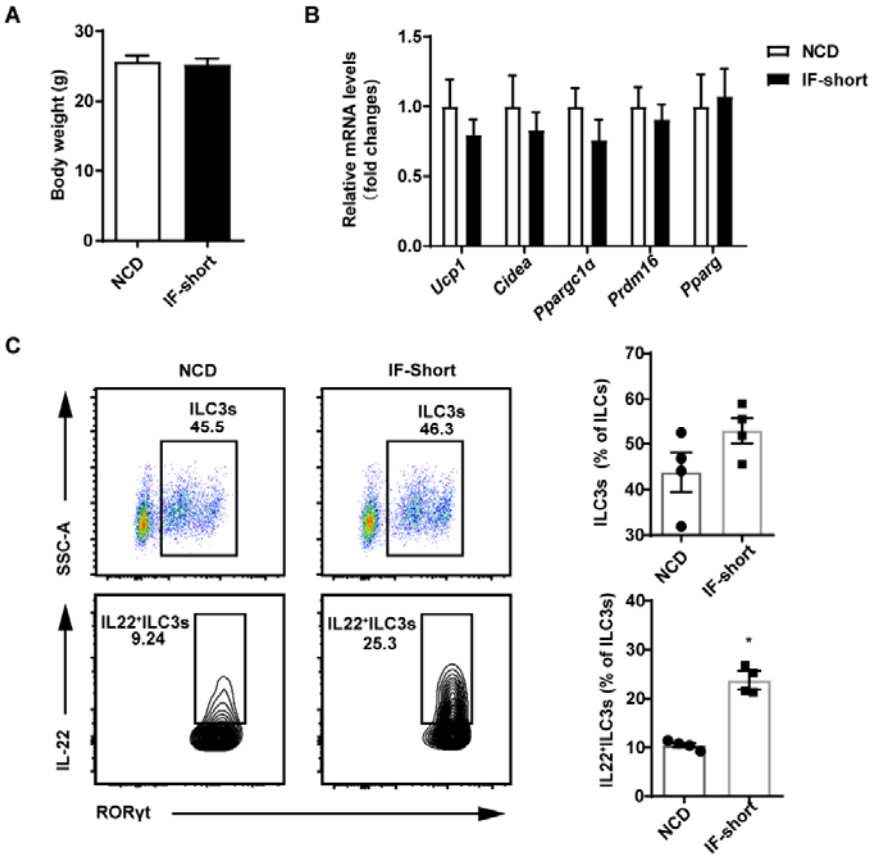

Figure 1—figure supplement 4 Short-term intermittent fasting induces intestinal ILC3s to secrete IL-22.

Eight-week-old SPF mice were exposed to one cycle of intermittent fasting for 2 days (IF-short), while the control group (NCD) has free access to NCD. n=6.

A. Body weight of NCD and IF-short mice. n=6.

B. qPCR analysis of thermogenic genes in sWAT from NCD and IF-short mice. n=6 mice/group.

C. Flow cytometric analysis of RORγt^{+} ILC3s in live CD127^{+} lineage^{-} ILCs in the small intestine lamina propria of NCD or IF-short mice. Flow cytometric analysis of IL-22^{+} cells in live CD127^{+} lineage^{-} RORγt^{+} ILC3s from the small intestine lamina

propria of NCD or IF-short mice. Four independent experiments were performed with similar results. n=4.

All data represent the mean ± s.e.m. Statistical significance was determined by unpaired two-tailed Student's *t* test.

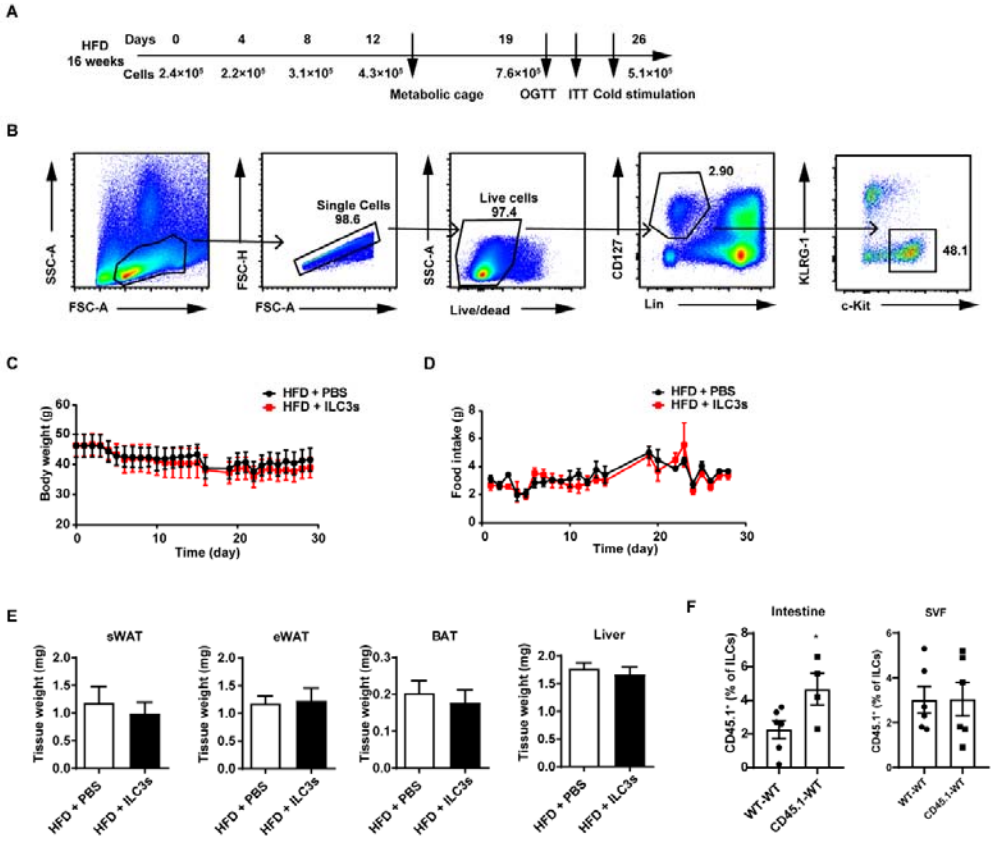

Figure 2—figure supplement 1 Adoptive transfer of ILC3s has no effect on the body weight in mice fed HFD.

A. Timeline for the recipient mice transferred with PBS or ILC3s. Mice were fed with HFD for 16 weeks and then injected with ILC3s intravenously six times in a month.

B. Gating strategy for flow sorting of live CD127^{+} lineage^{-} c-kit^{+} KLRG1^{-}ILC3s in the siLP.

C. Body weight of HFD mice transferred with ILC3s or control. n=6 per group.

D. Food intake of HFD mice transferred with ILC3s or control. n=6 per group.

E. Tissue weight of sWAT, eWAT, BAT, and liver from HFD mice transferred with ILC3s or control. n=6 per group.

F. Transfer of ILC3s from CD45.1 mice to WT mice. The percentage of CD45.1+ cells in ILCs in the small intestine and SVF. n=4-6.

All data represent the mean ± s.e.m. Statistical significance was determined by unpaired two-tailed Student's *t* test.

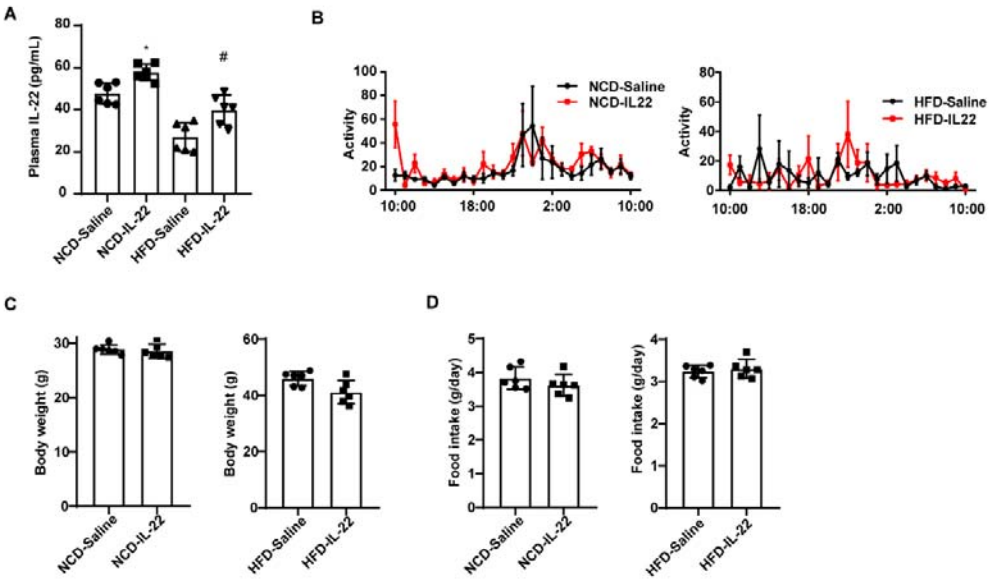

Figure 3—figure supplement 1 Exogenous IL-22 has no effect on the body weight of mice.

A. Levels of IL-22 in plasma of NCD-Saline, NCD-IL-22, HFD-Saline, HFD-IL-22 mice. n=6 mice/group. # vs HFD-Saline.

B. Activity of mice fed NCD or HFD which were intraperitoneally injected with IL-22

or saline. n=5 for each group.

C. Body weight of NCD and HFD mice intraperitoneally injected with IL-22 or saline. n=6 for each group.

D. Daily food intake of NCD and HFD mice intraperitoneally injected with IL-22 or saline. n=6 for each group.

E. qPCR analysis of *Il22ra1* genes in adipocytes or SVF cells isolated from sWAT. n=4. * denotes P<0.05 vs sWAT adipocytes.

F. qPCR analysis of adipogenic marker genes of SVF cells and adipocytes. n=3.

G. Relative protein signal intensity quantified using Image J software.

All data represent the mean ± s.e.m. Statistical significance was determined by one-way ANOVA (A) or unpaired two-tailed Student's *t* test (C, D).

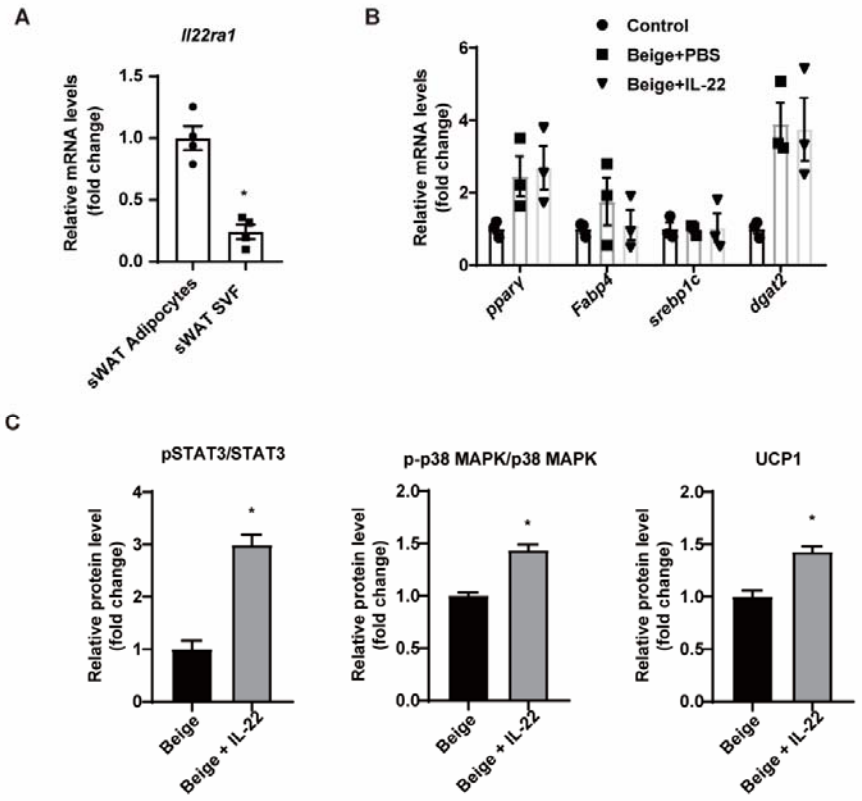

Figure 4—figure supplement 1 IL-22 can directly act on adipocytes.

A. qPCR analysis of *Il22ra1* genes in adipocytes or SVF cells isolated from sWAT. n=4. * denotes P<0.05 vs sWAT adipocytes.

B. qPCR analysis of adipogenic marker genes of SVF cells and adipocytes. n=3.

C. Relative protein signal intensity quantified using Image J software.

All data represent the mean ± s.e.m. Statistical significance was determined by one-way ANOVA (B) or unpaired two-tailed Student's *t* test (A, C).

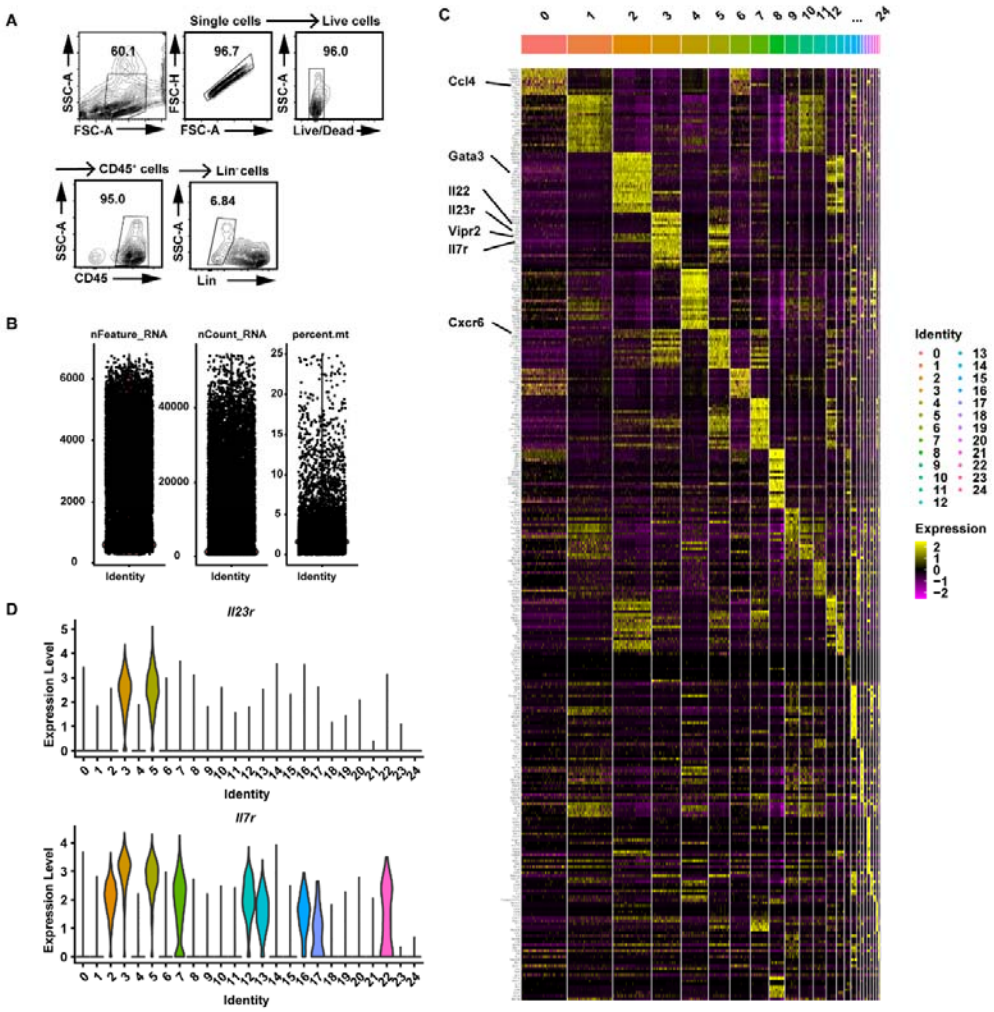

Figure 6—figure supplement 1 Profiling of intestinal immune cells from mice fed NCD, HFD or HFD-IF.

A. Gating strategy for flow cytometry sorting of Live CD45^{+} Lineage^{-} immune cells in the small intestine lamina propria.

B. scRNA-seq data quality control of sorted immune cells from mice fed NCD, HFD or HFD-IF.

C. Unbiased heatmap of the gene levels of the top 20 unique cluster marker genes for each cell cluster. Cluster identities are shown above the heatmap.

D. Violin plots showing RNA expression of cluster markers for the indicated cell

populations. UMAP feature plots are based on the UMAP shown in Figure 6A.

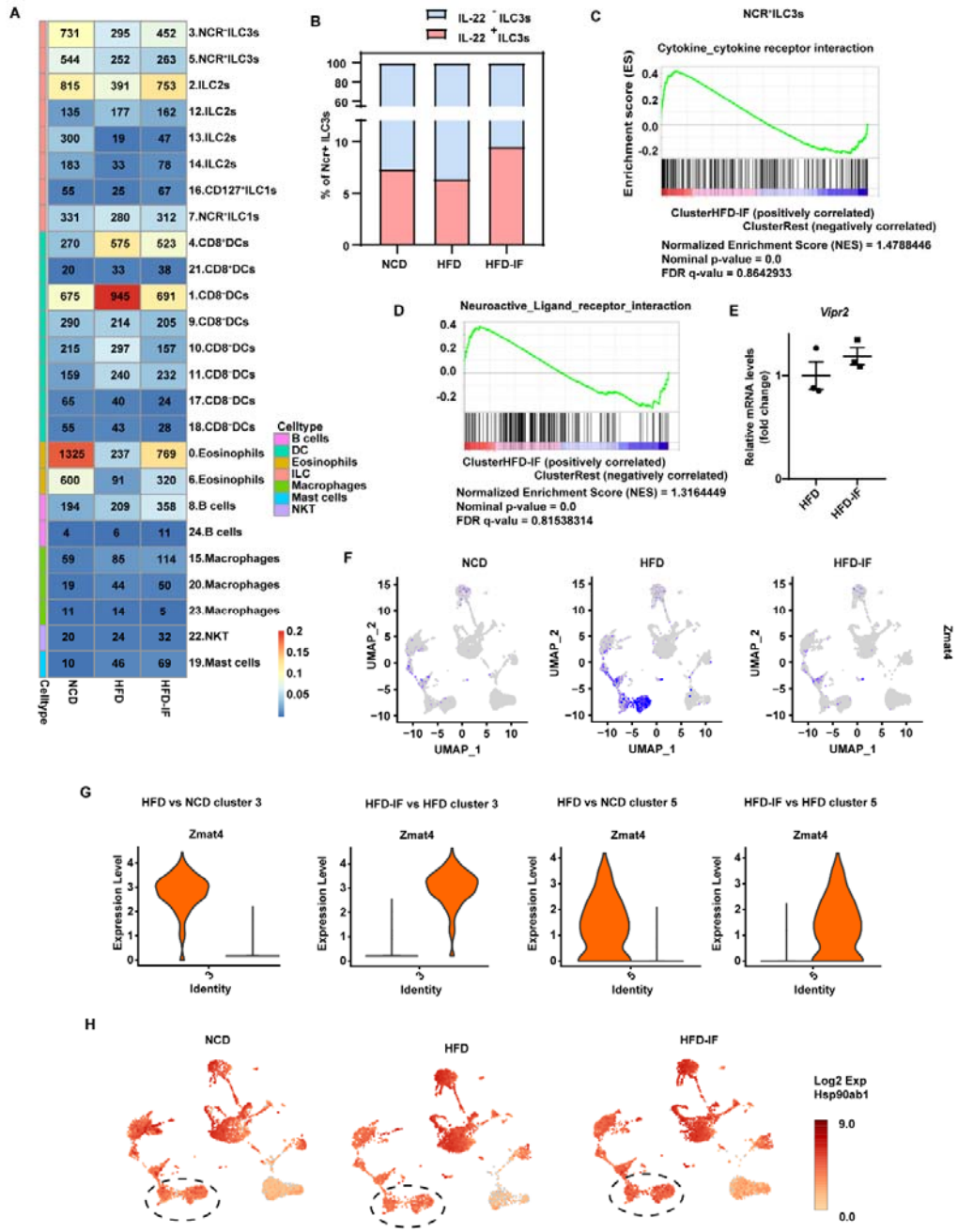

Figure 6—figure supplement 2 Effects of Intermittent fasting on the gene expression of ILC3s.

A. Number and proportion of cells detected in each group in the study. Shown are Fraction (color bar, out of all cells from that group) and number of cells from each of

the 25 cell clusters (rows) in each individual group (columns).

B. Percentage of IL-22^{+} cells defined by the mRNA levels using Loupe Browser 5.0 of NCR^{+} ILC3s in NCD, HFD and HFD-IF mice.

C. GSEA demonstrating enrichment of cytokine-cytokine receptor interaction pathway genes upregulated by intermittent fasting (HFD-IF mice) vs. control (HFD mice) in NCR^{+} ILC3s.

D. GSEA demonstrating enrichment of neuroactive ligand-receptor interaction pathway genes upregulated by intermittent fasting (HFD-IF mice) vs. control (HFD mice) in NCR^{+} ILC3s.

E. qPCR analysis of *Vipr2* in ILC3s sorted from siLP of HFD or HFD-IF mice.

F. UMAP feature plots showing RNA expression of Zmat4 based on the UMAP shown in Figure 6B.

G. Violin plots showing RNA expression of Zmat4 in NCR^{-}ILC3s (cluster 3) and NCR^{+}ILC3s (cluster 5).

H. UMAP feature plots showing RNA expression of Hsp90ab1 based on the UMAP shown in Figure 6B.

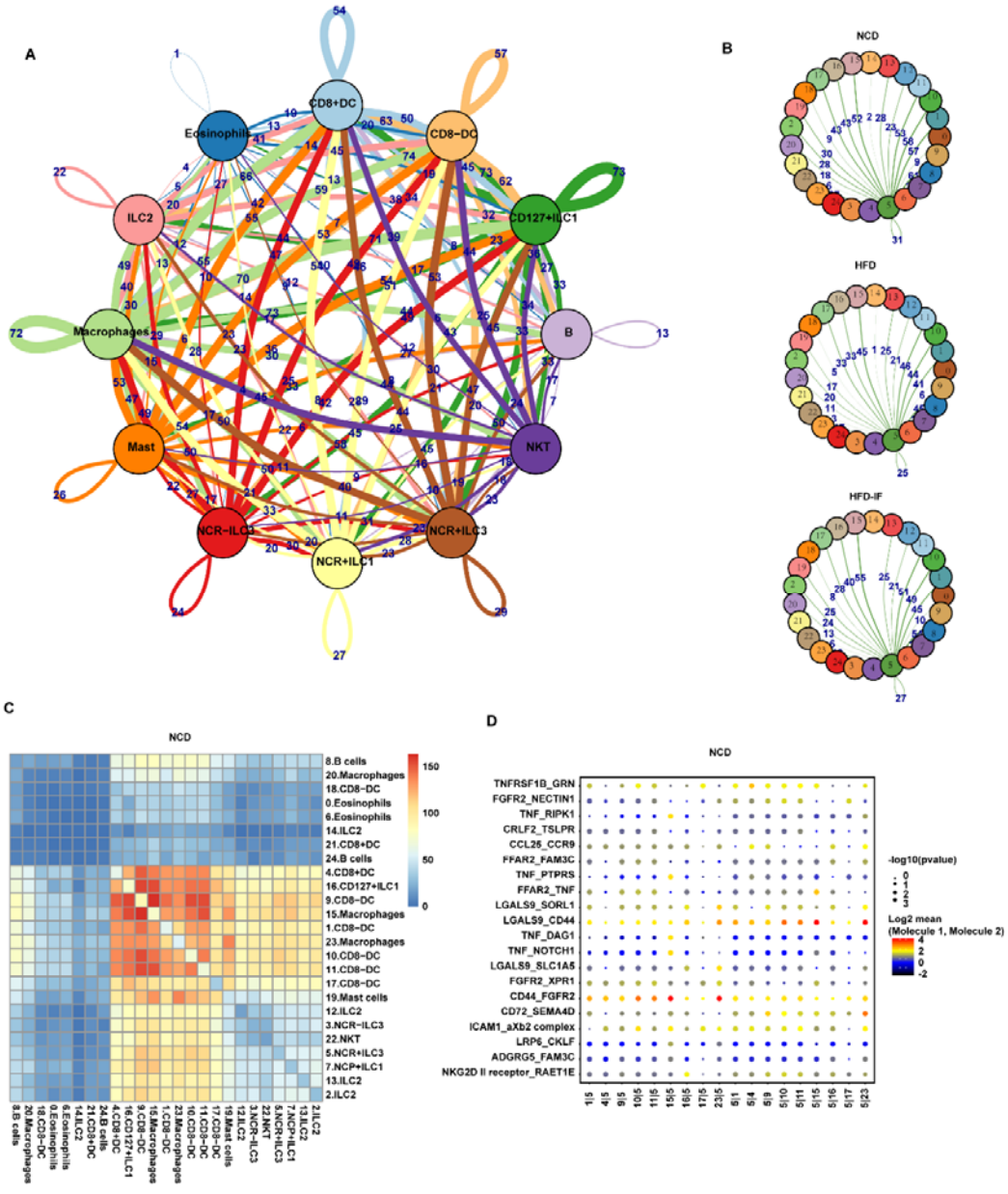

Figure 7—figure supplement 1 Cell–cell interactions in the intestine.

A. Connectome web analysis of intestine immune cell interacting cell types based on the expression of the ligand in mice fed NCD. The vertex (colored cell node) represents the cell cluster. The thickness of the connecting lines is proportional to the number of interactions between the nodes.

B. Connectome web analysis of NCR^{+} ILC3s with the 25 cell clusters based on

expression of the ligand. The vertex (colored cell node) represents the cell cluster, while the thickness of the connecting lines is proportional to the number of interactions between two nodes.

C. Heatmap showing the number of significant interactions identified between cell types in sorted siLP immune cells of NCD mice as determined by CellphoneDB. The color represents the number of interactions between cell types: a higher number of interactions (red) and a lower number of interactions (blue).

D. Interaction pattern of the top 20 protein pairs and the top 20 cell types. The x-axis is the cell type interaction, and the y-axis is the protein interaction. The larger the point is, the smaller the p value. The color represents the average expression. Red to black indicates the level from high to low.

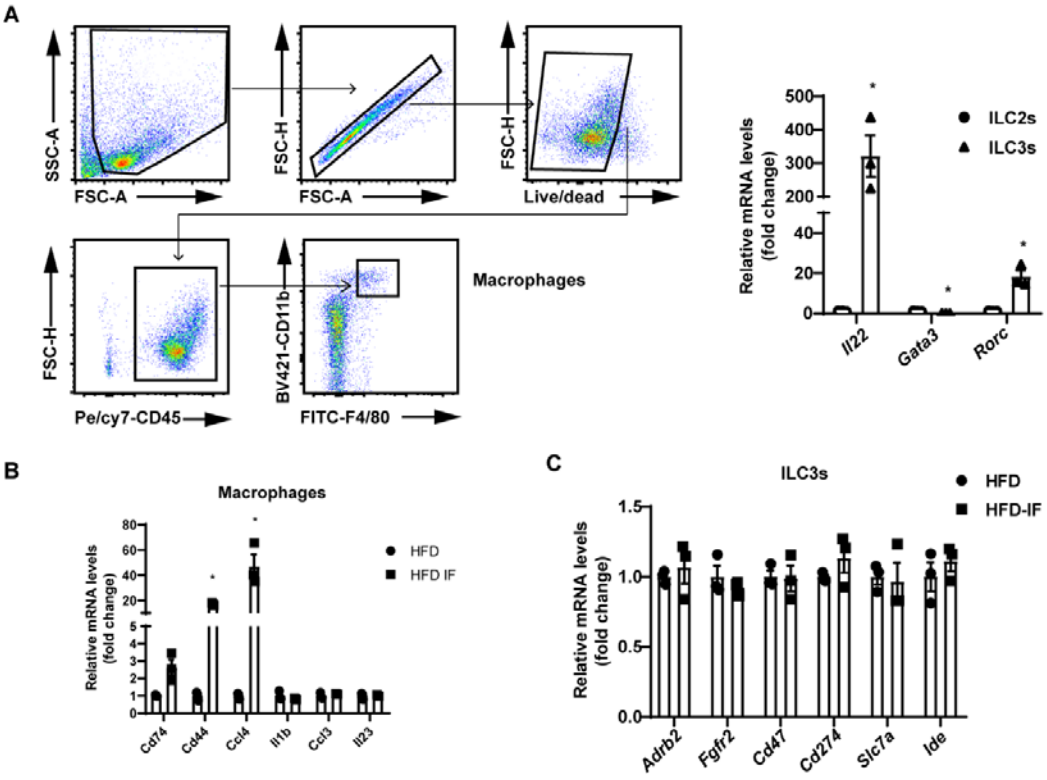

Figure 7—figure supplement 2 Increased expression of CD44 and CCl4 in

macrophages.

Flow cytometry sorted macrophages and ILC3s from HFD and HFD-IF mice were used to detect the mRNA levels of proteins involved in the interaction of macrophages and ILC3s.

A. Gating strategy for flow sorting of macrophages in the siLP. qPCR analysis of *Il22*, *Gata3*, and *Rorc* in ILC2s and ILC3s. n=3/group.

B. mRNA levels of proteins involved in the interaction and *Il23* in macrophages. n=3/group.

C. mRNA levels of proteins involved in the interaction in ILC3s. n=3/group.

All data represent the mean ± s.e.m. Statistical significance was determined by unpaired two-tailed Student's *t* test.

Supplementary File 1 Sequences of primers used in quantitative PCR.

Gene	**Forward Primer**	**Reverse Primer**
Il22	ATGAGTTTTTCCCTTATGGGGAC	GCTGGAAGTTGGACACCTCAA
Il17	TCCCTCTGTGATCTGGGAA	CTCGACCCTGAAAGTGAAGG
Il1β	CCTTCCAGGATGAGGACATGA	TGAGTCACAGAGGATGG-GCTC
Il6	TAGTCCTTCCTACCCCAATTTCC	TTGGTCCTTAGCCACTCCTTC
Ifnγ	ATGAACGCTACACACTGCATC	CCATCCTTTTGCCAGTTCCTC
Tbp	ACCTTATGCTCAGGGCTTGG	GCCGTAAGGCATCATTGGAC
RpL32	GAGCAACAAGAAAACCAAGCA	TGCACACAAGCCATCTACTCA
Hprt2	TCAGTCAACGGGGGACATAAA	GGGGCTGTACTGCTTAACCAG

Hsl	CCAGCCTGAGGGCTTACTG	CTCCATTGACTGTGACATCTCG
Adrb3	GGCCCTCTCTAGTTCCCAG	TAGCCATCAAACCTGTTGAGC
Chrebpβ	AGATGGAGAACCGACGTATCA	ACTGAGCGTGCTGACAAGTC
Dio2	AATTATGCCTCGGAGAAGACCG	GGCAGTTGCCTAGTGAAAGGT
Atp1a2	CCACCACTGCGGAAAATGG	GCCCTTAGACAGATCCACTTGG
Atgl	AACACCAGCATCCAGTTCAA	GGTTCAGTAGGCCATTCCTC
Fabp4	ACACCGAGATTTCCTTCAAACTG	CCATCTAGGGTTATGATGCTCTTCA
Cidea	ATCACAACTGGCCTGGTTACG	TACTACCCGGTGTCCATTTCT
Ppargc1α	GATTGAAGTGGTGTAGCGAC	GTCGCTACACCACTTCAATC
Pparg	TCAGCTCTGTGGACCTCTCC	ACCCTTGCATCCTTCACAAG
Adrb3	GGCCCTCTCTAGTTCCCAG	TAGCCATCAAACCTGTTGAGC
Prdm16	CAGCACGGTGAAGCCATTC	GCGTGCATCCGCTTGTG
Il4	GGTCTCAACCCCCAGCTAGT	GCCGATGATCTCTCTCAAGTGAT
Ucp1	CACCTTCCCGCTGGACACT	CCCTAGGACACCTTTATACCTAATGG
Il23a	ATGCTGGATTGCAGAGCAGTA	ACGGGGCACATTATTTTTAGTCT
Tnf	CGTCGTAGCAAACCACCAAG	GAGATAGCAAATCGGCTGACG
Adrb2	GGGAACGACAGCGACTTCTT	GCCAGGACGATAACCGACAT
Fgfr2	CCTCGATGTCGTTGAACGGTC	CAGCATCCATCTCCGTCACA
Cd47	TGGTGGGAAACTACACTTGCG	CGTGCGGTTTTTCAGCTCTAT
Cd274	GCTCCAAAGGACTTGTACGTG	TGATCTGAAGGGCAGCATTTC
Slc7a1	CTGCCTCAACACCTATGACCT	GAGAGCAGCAATCAAGAAGGAG
Ide	AATCCGGCCATCCAGAGAATA	GGGTCTGACAGTGAACCTATGT

Cd74	AGTGCGACGAGAACGGTAAC	CGTTGGGGAACACACACCA
Cd44	TCGATTTGAATGTAACCTGCCG	CAGTCCGGGAGATACTGTAGC
Ccl4	TTCCTGCTGTTTCTCTTACACCT	CTGTCTGCCTCTTTTGGTCAG
Il1b	GCAACTGTTCCTGAACTCAACT	ATCTTTTGGGGTCCGTCAACT
Ccl3	TTCTCTGTACCATGACACTCTGC	CGTGGAATCTTCCGGCTGTAG
Gata3	CTCGGCCATTCGTACATGGAA	GGATACCTCTGCACCGTAGC
Rorγt	GACCCACACCTCACAAATTGA	GACCCACACCTCACAAATTGA